Schweizerische Eidgenossenschaft
Confédération suisse
Confederazione Svizzera
Confederaziun svizra

**Final report dated** 6 December 2019

# Direkte Numerische Simulation und experimentelle Validierung der Zündung/Entflammung und der Wand-/Flammeninteraktion in zukünftigen Gasmotoren

# Direct Numerical Simulation and experimental validation of ignition/early flame propagation and flame-wall interactions in future gas engines

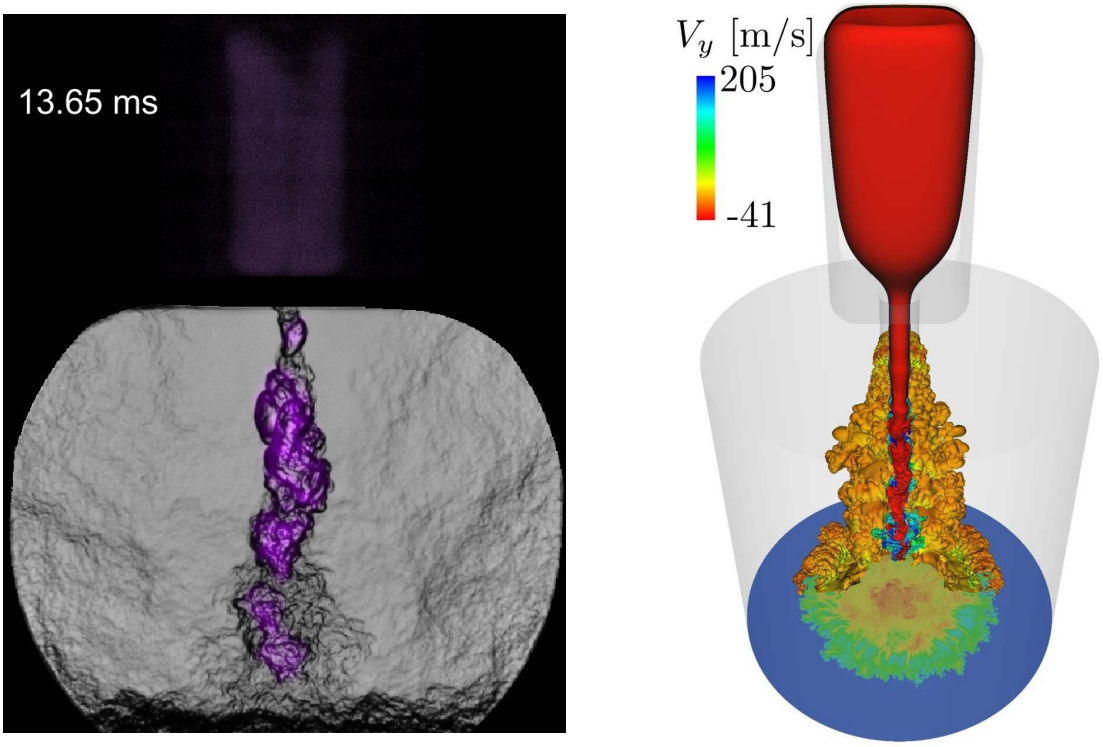


**Source:** Left image: A. Denisov and P. Kyrtatos, right image: S. Benekos, G. Giannakopoulos and C.E. Frouzakis

**Date:** 6.12. 2019
**Location:** Zurich

**Subsidiser:**
Swiss Federal Office of Energy SFOE
Energy Research and Cleantech Section
CH-3003 Bern
www.bfe.admin.ch

**Co-financing**
- KTI/CTI, Einsteinstrasse 2, 3003 Bern
- Liebherr Machines Bulle SA, rue de l'Industrie 45, Postfach 272, 1630 Bulle, FR
- EU H2020 project GasOn, Grant Agreement Number 652816, www.gason.eu

**Subsidy recipients:**
ETH Zürich, Institut für Energietechnik
Laboratorium für Aerothermochemie und Verbrennungssysteme
Sonneggstrasse 3
CH-8092 Zürich

**Authors:**
Sotirios Benekos, Aerothermochemistry and Combustion Systems Laboratory,
ETH Zürich, benekos@lav.mavt.ethz.ch
Dr. Christos E. Frouzakis, Aerothermochemistry and Combustion Systems Laboratory,
ETH Zürich, frouzakis@lav.mavt.ethz.ch
Dr. Georgios Giannakopoulos, Aerothermochemistry and Combustion Systems Laboratory,
ETH Zürich, georgeg@lav.mavt.ethz.ch
Dr. Yuri M. Wright, Aerothermochemistry and Combustion Systems Laboratory,
ETH Zürich, wright@lav.mavt.ethz.ch
Dr. Michele Bolla, Aerothermochemistry and Combustion Systems Laboratory,
ETH Zürich, mbolla@lav.mavt.ethz.ch
Dr. Panos Kyrtatos, Aerothermochemistry and Combustion Systems Laboratory,
ETH Zürich, kyrtatos@lav.mavt.ethz.ch
Dr. Bruno Schneider, Aerothermochemistry and Combustion Systems Laboratory,
ETH Zürich, schneider@lav.mavt.ethz.ch
Dr. Alexey Denisov, Institute of Thermal and Fluid Engineering of the University of Applied Sciences and Arts Northwestern Switzerland (FHNW), alexey.denisov@fhnw.ch
Prof. Kai Herrmann, Institute of Thermal and Fluid Engineering of the University of Applied Sciences and Arts Northwestern Switzerland (FHNW), kai.herrmann@fhnw.ch
Prof. Konstantinos Boulouchos, Aerothermochemistry and Combustion Systems Laboratory, ETH Zürich, boulouchos@lav.mavt.ethz.ch

**SFOE project coordinators:**
Dr. Carina Alles, Carina.Alles@bfe.admin.ch
Stephan Renz, renz.btr@swissonline.ch
**SFOE contract number:** SI/501301-01 / 8100075

# Zusammenfassung

In diesem Projekt wurden die grundlegenden Prozesse in Vorkammerzündsystemen untersucht. Solche Zündsysteme werden in mageren Erdgasmotoren eingesetzt, um die Verbrennungsrate zu erhöhen und zyklische Schwankungen zu reduzieren. Dabei ist die Vorkammer über kleine Überströmbohrungen mit der Hauptbrennkammer verbunden. Der Druckanstieg durch die Verbrennung erzeugt heisse, reaktive, turbulente Strahlen in der Hauptkammer, die deutlich höhere Zündenergie liefern und verteilte Zündstellen erzeugen. Dies führt zu einer intensivierten und beschleunigten Verbrennung, minimiert die Variabilität von Zyklus zu Zyklus und ermöglicht eine höhere Abmagerung bei gleichzeitiger Verringerung der Menge an unverbrannten Kohlenwasserstoffen im Abgas.

Aufgrund des schnellen transienten Wechselwirkung zwischen Turbulenz und chemischer Kinetik, welche stark von der komplexen Geometrie und den Betriebsbedingungen beeinflusst wird, sind die grundlegenden Prozesse bei der Verbrennungsinitiierung in der Vorkammer und das anschließende Eindringen der heissen reaktiven Strahlen in die Hauptkammer, welche zum Verbrennen der Hauptladung führen, noch nicht vollständig verstanden. Zur detaillierten Untersuchung der Vorgänge wurde in diesem Projekt deshalb ein neuer Prüfstand entwickelt und gebaut, der einen optischen Zugang zu beiden Kammern ermöglicht und mit Sensoren zur Messung der Wärmeflüsse an den Wänden ausgestattet ist. Messungen wurden bei unterschiedlichen Drücken, Temperaturen und Gaszusammensetzungen mit Düsen mit unterschiedlichen Durchmessern durchgeführt. Parallel zu den Experimenten wurden Direkte Numerische Simulationen (DNS) durchgeführt. Die Kombination ermöglicht einzigartige Einblicke in die physikalischen und chemischen Prozesse als auch detaillierte Daten für die Validierung und Abstimmung bestehender Modelle in CFD Codes sowie für die Entwicklung neuer Modelle. Die Dynamik der transienten zunächst kalten und anschließend reaktiven Strahlen und deren Aufbruch, welche die Zündung und den Verbrennungsmodus in der Hauptkammer bestimmen, wurde genau erfasst und die umfangreichen, hochdetaillierten Datensätze werden derzeit nachbearbeitet. Die Analyse der Daten wird nach Abschluss des Projekts fortgesetzt.

# Summary

Prechamber ignition systems are used in lean-burn natural gas engines to increase combustion rate and reduce cyclic variations. In such systems, the prechamber is connected with the main combustion chamber through small orifices. The pressure increase due to combustion creates hot reactive turbulent jets in the main chamber, providing significantly higher ignition energy and creating distributed ignition sites. This leads to intensified and accelerated combustion, minimizing cycle-to-cycle variability, and allows for increased dilution levels while diminishing the amount of unburned hydrocarbons in the exhaust.

Due to the fast transient interaction of turbulence and chemical kinetics which is strongly affected by the complex geometry and the operating conditions, the fundamental processes during combustion initiation in the pre-chamber and the subsequent penetration of the hot reactive jets into the main chamber leading to the burning of the main charge are not yet fully understood. In this project, a combination of optical diagnostics in a novel optically-accessible generic pre- and main chamber setup with direct numerical simulations (DNS) provide both unique insights into the physical and chemical processes and detailed data for the validation and tuning of existing models in engineering codes as well as for the development of novel models.

A new test rig was designed and manufactured, which provides optical access to both chambers and is equipped with sensors to measure heat fluxes to the walls. Measurements were performed for different pressures, temperatures, and compositions in the two chambers using nozzles of different diameter. Parametric two-dimensional (2D) DNS highlighted the importance of geometric, initial thermochemical state and operating conditions, and provided insights into flame propagation in the

prechamber, and the flow and mixing driven first by the cold jet which becomes turbulent by the time the flame front reaches the nozzle exit, and subsequently into the ignition and consumption of the main chamber charge. Computationally demanding 3-D DNS were performed in two setups: (i) a simplified setup where the effect of the prechamber was mimicked by appropriately choosing the time-varying inflow velocity, temperature and composition profiles, and (ii) the experimental geometry, albeit with a smaller diameter of the main chamber cylinder. The dynamics of the transient initially cold and subsequently reactive jets and their breakup that determine the ignition and mode of combustion in the main chamber were accurately captured and the rich datasets that were generated are currently post processed. The analysis of the large scale data will continue after the end of the project.

# Main accomplishments

- Experimental investigation of the effect of initial pressure and temperature, composition in the pre- and main chamber, and nozzle diameter on the progress (via pressure measurements in both chambers) and mode of combustion (via Schlieren and OH* chemiluminescence imaging using a 200 kHz camera) in a state-of-the-art novel setup.
- Physical understanding of the physical and chemical processes through capturing of the evolution of the flow, temperature and composition using highly resolved direct numerical simulations in laboratory-scale setups, and quantitative characterization of the processes and their interactions.
- Experimental and numerical data for validation of the the RANS and LES CFD setups developed during the project and to support the development and validation of fast quasi-dimensional models based on first principles.

# Contents

# Abbreviations

| | |
|---|---|
| CFD | Computational Fluid Dynamics |
| CLA | cold lean adiabatic (condition specification for 2D DNS) |
| CSA | cold stoichiometric adiabatic (condition specification for 2D DNS) |
| HLA | hot lean adiabatic (condition specification for 2D DNS) |
| HSA | hot stoichiometric adiabatic (condition specification for 2D DNS) |
| DT | delay time |
| DNS | Direct Numerical Simulation |
| LES | Large Eddy Simulation |
| HRR | heat release rate |
| IDT | ignition delay time |
| iHRR | integral heat release rate |
| MC | main chamber |
| PC | prechamber |
| OPC | optical prechamber |
| SDR | scalar dissipation rate |

# 1 Introduction

## 1.1 Background information and current situation

Due to its low carbon content, natural gas (NG) has considerable potential as a cleaner fuel for internal combustion engines (ICEs). Depending on the source (compressed or liquified vs. renewable NG), it can provide significant life cycle greenhouse gas emission benefits. Additional advantages include its availability, soot-free combustion and strong antiknock properties, which allow for high compression ratios and thus increased thermal efficiency and reduced fuel consumption [1, 2].The emissions level of ICEs depends on the characteristics of natural gas, the operating conditions, the combustion chamber design, and spark timing. Lean combustion strategies can additionally offer higher thermal efficiency, lower fuel consumption, and lower operating temperature leading to less NOx emissions, but may lead to unstable operation including misfire.

In order to exploit the advantages of lean NG combustion, the low flame speed which results in long combustion duration, the misfire and low ignitability due to leaning have to be addressed. Apart from the conventional spark, different ignition systems have attracted increasing attention recently. These include plasma igniters [3], laser-induced ignition [4] pilot ignited duel-fuel concepts [5, 6], and prechamber (PC) ignition systems. The turbulent jet ignition (TJI) observed in the latter is described in the review papers [7, 8] and the references therein. PC ignition systems have been proposed as an alternative to spark ignition due to their ability to sustain stable and successful combustion of very lean mixtures [9-11], with the potential to decrease unburned hydrocarbons and CO emissions [7, 12, 13]. Compared to spark plugs, PC ignition have been reported to offer the potential for five- to seven-fold reduction in ignition delay time (IDT), a three- to four-fold reduction in combustion duration and enables a wider range of lean mixtures combustion by a factor of 1.5 to 2 leading to reduced fuel consumption [9, 14], while $NO_x$ emissions are low because of the low combustion temperature [15]. The key component of the system is a small auxiliary prechamber attached at the top or side of the main engine combustion chamber, where a typically richer mixture is ignited by a spark plug. The hot gas produced by combustion in the PC exits into the main chamber (MC) through one or more orifices as turbulent reacting jet(s), providing favorable local mixing and rapid combustion throughout the main chamber.

Understanding of the processes in such a setup and their complex interactions is crucial for the design of turbulent jet ignition systems. The flow and combustion are tightly coupled and are affected by geometric design parameters (volume ratio of the pre- to the main chamber, arrangement and shape, nozzle diameter, number of orifices etc.), and operating conditions (equivalence ratio in the two chambers, turbulence generated within the PC before spark ignition and by the hot transient, reactive jets exiting the prechamber etc.).

On the experimental side, studies in rapid compression machines [16, 17], divided-chamber and connected setups [18-23], or measurements in engines [7, 9-12, 24, 25] have been conducted to investigate different prechamber designs and conditions. However, the difficulty to access near-wall regions and the limited options for accessing the small PC volumes restrict the use of non-intrusive laser diagnostics, and measurements can only provide partial information of the system state. On the numerical side, investigations of TJIs have been conducted using Numerically efficient quasi-dimensional [26, 27], Reynolds-Averaged Navier-Stokes (RANS) [16, 17, 28-30], and Large Eddy Simulations (LES) [31-35]. Three-dimensional detailed numerical simulations are rare [36] and limited to a narrow range of initial thermochemical conditions due to their high computational cost.

## 1.2 Purpose of the project

The performance of prechamber ignition systems depends sensitively on the interaction of different processes as well as on the design and operating conditions. All these result in a combustion behavior that changes locally depending on the local flow and mixing conditions, which are crucially affected by the flow generated by the prechamber itself as well as by the structure and stability of the flame exiting the nozzle connecting the two chambers. In order to investigate the challenging physics of both the generation of the turbulent hot jet and the subsequent ignition and fuel consumption of the main chamber charge, the project combines experiments in a novel state-of-the-art set up with optical access to both the pre- and main chamber with detailed numerical simulations that provide accurate description of the spatial and temporal evolution of all variables of interest (flow velocity, temperature and chemical composition).

## 1.3 Objectives

In-depth understanding of combustion in gas engines through optical diagnostic experiments and direct numerical simulations, which resolve accurately all relevant length and time scales. Based thereupon evaluation of appropriate models for industrial applications towards development of future gas engines with ultra-low $CH_4$ emissions. The focus is on three main areas: early flame propagation within the pre-chamber, flame stability at the entrance to the main combustion chamber and influence of the walls on flame propagation and fuel consumption.

# 2 Procedures and methodology

## 2.1 Experimental investigations

A new Optically-accessible Pre-Chamber (OPC) was designed, manufactured, and installed in the optical laboratory of LAV in ETH Zurich. A view of the whole test-rig, including all peripherals, is shown in **Figure 1**.

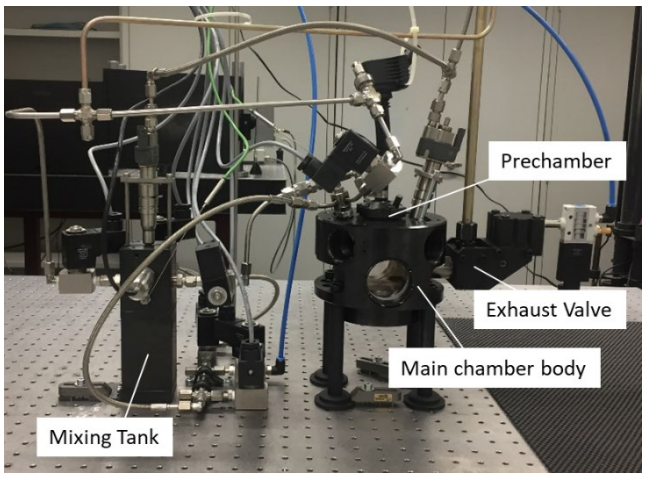


**Figure 1. View of the experimental facility, with the major components indicated.**

Views of the optical access into the pre- and main chambers can be seen in **Figure 2**. In the prechamber view, the spark plug secondary electrode protruding into the chamber is visible; optical accessibility

allows the observation of the early flame development. In the main chamber view, the chamber top as well as the opposing wall can be seen.

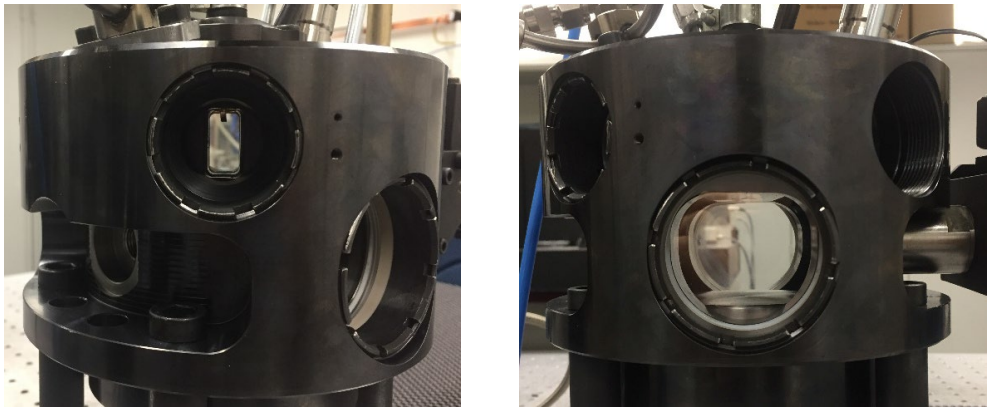

**Figure 2. Views of the optical access into the prechamber (left) and the main chamber (right).**

Several measurement campaigns were performed, which included Schlieren and OH* chemiluminescence imaging of the flame propagation in the prechamber and main chamber, pressure measurement in both chambers, and heat flux measurements at points on the lower and a prechamber wall in a collaboration between LAV and the Institute of Thermal and Fluid Engineering of the University of Applied Sciences and Arts Northwestern Switzerland (FHNW).

In order to study the repeatability of mixture preparation, ignition and flame propagation in the prechamber, the pressure rise after ignition in multiple cycles with constant settings was recorded. In this experimental setup the filling of the prechamber takes place prior to ignition, using a fuel/air mixture which is prepared in an external mixing device (indicated as the mixing tank in **Figure 1**). The device allows to set a different mixture in the prechamber and the main chamber prior to ignition, enabling the emulation of ignition in a scavenged prechamber engine.

In order to achieve high repeatability, the mixture in the mixing tank is prepared once for each set of measurements, and repetitions of the same point are conducted until the mixing tank pressure becomes insufficient to conduct further experiments. The parameter which was optimized for high repeatability was the amount of mixture which was transferred from the mixing tank to the prechamber prior to ignition. This quantity was set to six times the prechamber volume, which was found to be sufficient for very repetitive prechamber combustion. **Figure 3** shows exemplarily the pressure difference between the two chambers resulting from combustion, for multiple repetitions at constant conditions. The two figures differ in the initial unburned mixture temperature (left: $T_u$=300K; right: $T_u$=430K), resulting in the observable difference in the rate of increase of the prechamber pressure. Under all conditions, the pressure difference showed low deviation from the mean for successive repetitions with constant conditions.

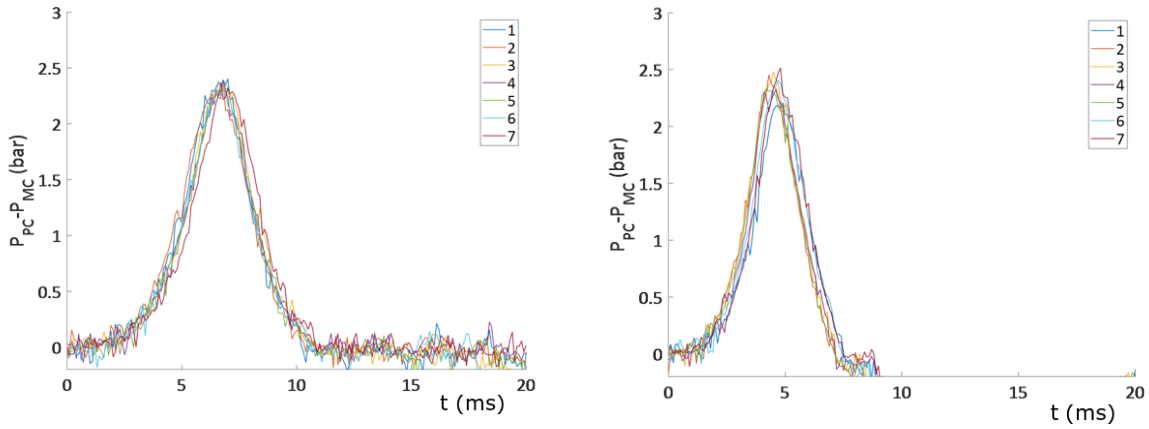


**Figure 3. Pressure difference between pre- and main chamber for seven repetitions at constant conditions with low (left, 300K) and high (right, 430K) initial charge temperature, $d_j$=2 mm nozzle, 5 bar initial pressure and $\varphi_{PC}$=1.0.**

## 2.2 Numerical investigations

### 2.2.1 Direct numerical simulations

The direct numerical simulations of the optical prechamber were performed using the computationally-efficient high-order spectral element solver for low Mach number combustion developed at LAV that is based on the open-source flow solver Nek5000. Two- and three-dimensional simulations were performed using a 20-species, 96-reactions skeletal mechanism to describe the kinetics of combustion and detailed transport. The skeletal mechanism was constructed using the entropy production analysis [37] starting from the commonly used GRI-3.0 detailed reaction mechanism [38] for natural gas combustion. The simulations were performed mainly at the Swiss Supercomputing Center (CSCS) using the allocation of the project “s753 - Investigation of prechamber-induced ignition of natural gas using direct numerical simulations” acquired specifically for this project with a dedicated proposal.

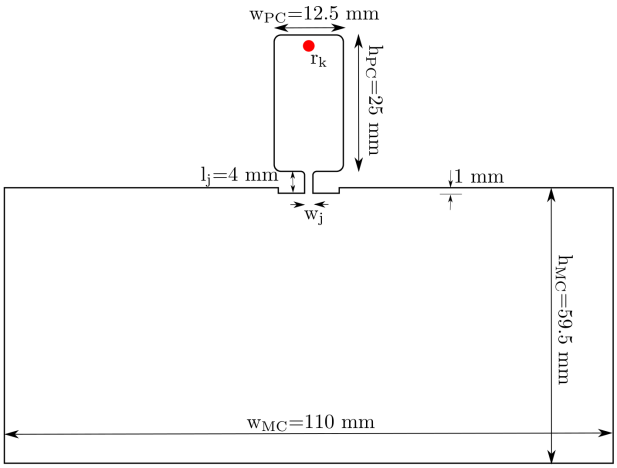


**Figure 4. Schematic of the geometry used in the two-dimensional DNS.**

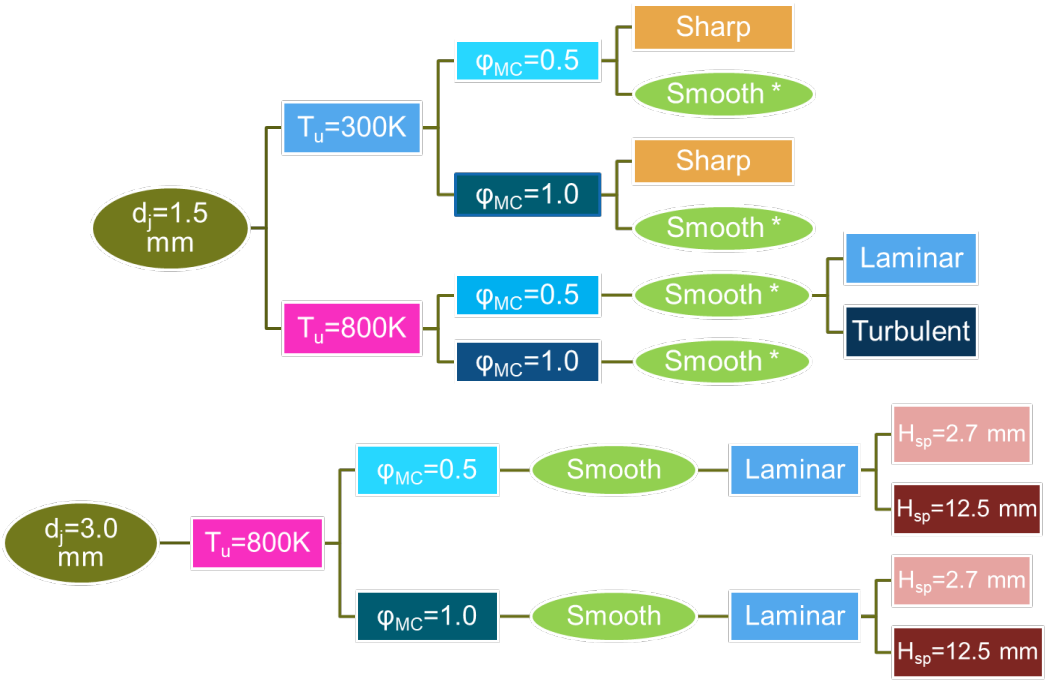


**Figure 5. Matrix of the 15 two-dimensional simulations. All cases considered fixed wall temperature ($T_w$=500K) except those marked by a star (*) for which both constant $T_w$=$T_u$ and adiabatic wall boundary conditions were imposed.**

The parametric 2-D simulations were performed in a computational domain that consists of a 12.5 x 25 mm$^2$ prechamber (PC) connected via a nozzle with a width of either $w_j$=1.5 or 3.0 mm to the 110 x 50.5 mm$^2$ main chamber (MC); the nozzle entry has either sharp or smoothed corners (**Figure 4**). The investigated conditions are graphically summarized in **Figure 5**. It should be noted that these simulations were performed before the design and construction of the OPC was finalized, and the high temperature condition differs from what can be experimentally achieved. An ignition kernel placed at either $H_{sp}$=2.7 mm or 12.5 mm away from the upper PC wall was used to ignite the mixture and initiate the flame in the PC. The domain is discretized in 60,415 spectral elements with polynomial order N=10, amounting to approximately 60.4 million grid points at which the evolution of the 24 flow and thermo-chemistry variables is computed, resulting in 1.45 billion unknowns and a computational cost ranging between 110 and 160 kCPUhr per case.

Two setups were considered in the 3-D simulations. The first was a simplified setup consisting of only the nozzle and the main chamber was employed to decrease the very high computational cost while preserving the main physics observed in the 2-D simulations. The reduced computational cost also enables the DNS at higher pressure. The role of the prechamber is emulated by imposing time-dependent velocity, temperature and composition profiles at the inflow (**Figure 6**(b)). During the initial 0.4 ms, the unburned mixture with a temperature T=800 K and pressure p=5 atm flows into the main chamber containing a lean premixed methane/air mixture at $T_{MC}$=800 K and p=5 atm with an inflow velocity of $V_{in}$=100 m/s in order to generate local flow and mixing conditions which are similar to the experimental setup. During the next phase, a mixture at thermodynamic equilibrium containing all the species accounted for in the reaction mechanism is fed at the inflow with the inlet velocity quickly ramped up to $V_{in}$=200 m/s to emulate the ejection of the hot reactive jet from the PC, kept constant for 2 ms, and finally linearly reduced to zero, emulating the complete combustion of the PC mixture.

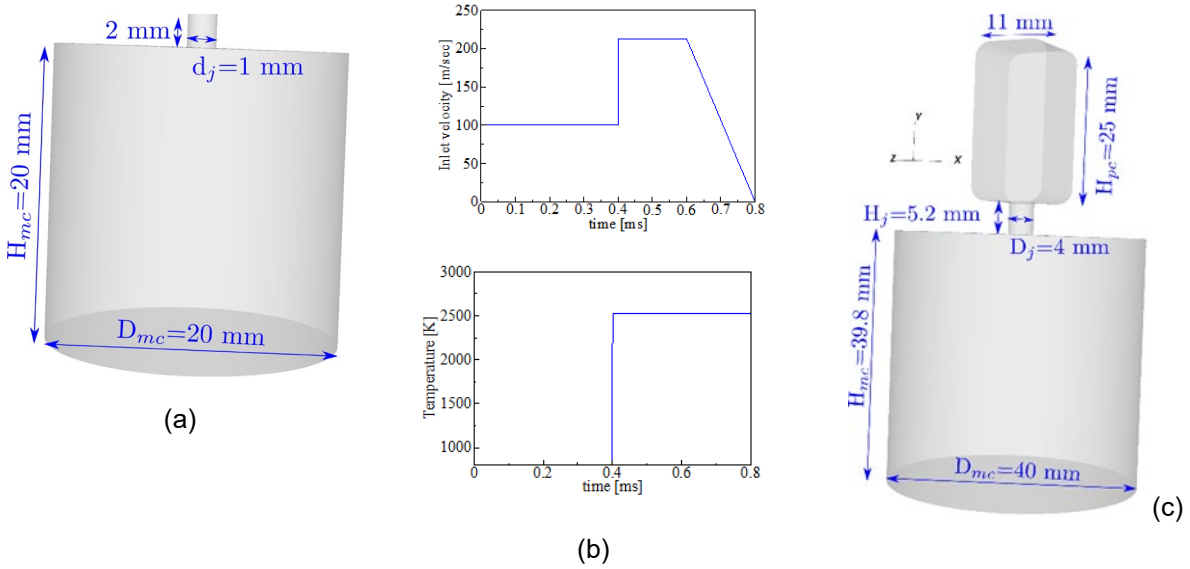


**Figure 6. (a) Schematic of the simplified 3-D setup; temporal variation of (b) the maximum velocity and temperature at the nozzle inlet, and (c) schematic of the experimental OPC setup.**

The second 3-D setup is that of the experiment, albeit with a smaller main chamber. Since due to computational cost the focus is on the initial phase of fuel consumption in the main chamber, the pressure increase will be only slightly affected by the reduction in size and the associated effect on reactivity will remain weak. With the exception of the main chamber, which was reduced to a cylinder of diameter $D_{mc}$=40 mm, the geometry has the dimensions of the experimental facility (**Figure 6**(c)). The stoichiometric $CH_4$/air mixture in the PC and the $\varphi_{MC}$=0.75 mixture are initially at $T_u$=450 K and p=1 atm.

It is also worth pointing out that a number of additional DNS studies were initiated to investigate separately different phenomena which were found to be of importance based on the physical understanding obtained from the DNS. These preliminary studies were performed during semester and bachelor thesis projects at LAV, and include the effects of nozzle diameter on flame propagation in narrow gaps for freely and forced flame propagation (imposed inflow velocity), as well as of the products of partial combustion in the prechamber. The DNS results are also used to guide development and to validate the quasi-dimensional models at LAV.

### 2.2.2 Reynolds Averaged and Large Eddy Simulations

The whole setup is too large and the associated cost for 3-D direct numerical simulations makes parametric investigations impractical. Instead, we initiated the study of the complete volume of the experimental setup and conditions using the RANS and LES models implemented in the commercial code CONVERGE CFD, which solves the averaged or filtered equations using locally and adaptively refined meshes.

# 3 Results and discussion

## 3.1 Experimental investigations

The measurements concentrated on the development of understanding of ignition of the main chamber mixture under different thermochemical conditions in the pre- and main chambers, and with different nozzle diameters. To accomplish this, experimental campaigns were conducted, which included measurements with variations of initial charge pressure, temperature, main chamber equivalence ratio and nozzle diameter, while keeping the fuel ($CH_4$) and prechamber equivalence ratio ($\varphi_{PC}$=1.0) fixed. A typical set values are provided in **Table 1**, where the reference conditions for the measurement is highlighted in blue, while the varying parameters for each measurement point compared to the reference are highlighted in purple.

**Table 1: Experimental campaign measurement set points, showing the reference measurement (blue) and the variations in parameters (purple).**

| Initial Pressure bar | Initial Temperature K | $\phi_{MC}$ | $\phi_{PC}$ | $d_j$ mm |
|---|---|---|---|---|
| 5 | 298 | **1** | 1 | 4 |
| **5** | **298** | **0.75** | **1** | **4** |
| 5 | 298 | **0.6** | 1 | 4 |
| **1** | 298 | **1** | 1 | 4 |
| **1** | 298 | 0.75 | 1 | 4 |
| **1** | **450** | **1** | 1 | 4 |
| **1** | **450** | 0.75 | 1 | 4 |
| **1** | **450** | **0.6** | 1 | 4 |
| 5 | 298 | **1** | 1 | **2** |
| 5 | 298 | 0.75 | 1 | **2** |
| 5 | 298 | **0.6** | 1 | **2** |
| 5 | **450** | **1** | 1 | **2** |
| 5 | **450** | 0.75 | 1 | **2** |
| 5 | **450** | **0.6** | 1 | **2** |
| 5 | **450** | **0** | 1 | **2** |

In the interest of conciseness, the following will focus on three of these 15 measurement points. This subgroup is used to shed light into the flame quenching and re-ignition phenomena observed. In addition to the reference point (blue), the two conditions marked in red in Table 1 were considered, where the nozzle diameter and charge temperature are varied. The actual measured average values for the three points considered are provided in **Table 2**.

**Table 2: Experimental campaign measurement set points, showing the reference measurement (blue) and the variations in parameters (purple).**

| Case | Initial pressure, bar | Initial temperature, K | $\phi_{MC}$ | $\phi_{PC}$ | Nozzle diameter, mm | Fuel |
|---|---|---|---|---|---|---|
| **1** | **5.67** | **302** | **0.75** | **0.97** | **4** | **CH4** |
| 2 | 5.13 | 299 | 0.75 | 0.92 | **2** | CH4 |
| 3 | 5.16 | **434** | 0.74 | 0.94 | **2** | CH4 |

The experimental results for these cases are presented in the figures below. **Figure 7** shows the measured main chamber pressure (blue, left axis), together with the pressure difference between main chamber and prechamber (red, right axis), plotted against time after spark. All five or seven repetitions are plotted for each case.

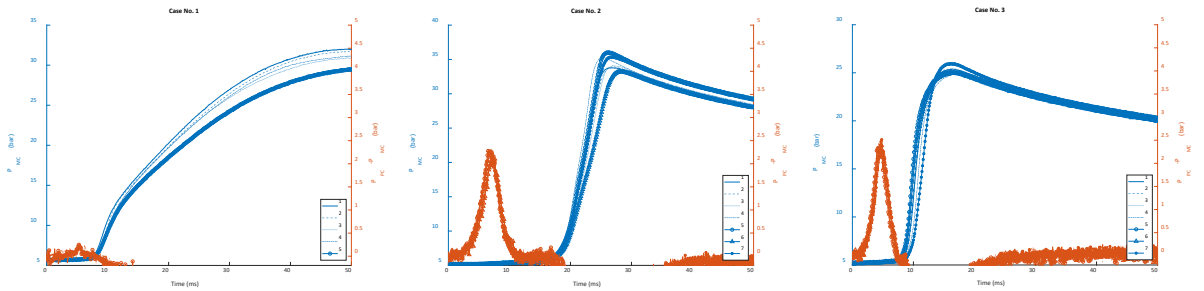


**Figure 7. Measured main chamber pressure (blue, left axis) and prechamber minus main chamber pressure difference (red, right axis) plotted over time after ignition for all repetitions of the OPC.**

**Figure 8** shows Schlieren images from the main chamber superimposed with the OH* chemiluminescence (purple) for characteristic time instants for each of the three cases. The images are taken from a representative repetition of the experiment, chosen as the case with pressure closest to the average of all measurements at the same conditions. Note that the time instances differ, since the timings of the hot jet exit and subsequent ignition differ significantly. Also note that the OH* is only shown as a binary value above a certain arbitrary threshold, which is chosen to remove signal noise. This value allows comparison of the locations of significant OH* luminosity, permitting the determination of reaction zones and enabling identification of flame quenching and re-ignition.

In case 1, minimal pressure increase is observed in the prechamber (**Figure 7**(a)), while the main chamber ignites very quickly after the hot jet exit. The burned products are first observed in the main chamber at 5.5 ms after the spark, with some OH* visible immediately. The hot jet then penetrates into the main chamber and impinges on the opposing wall, with the tip of the jet showing no OH* signal, indicating flame quenching, possibly due to mixing. The main chamber pressure shows significant increase only after 7.2 ms, which is also where a broader OH* signal is observed.

In cases 2 and 3, the pressure increase in the prechamber is much higher, due to the lower cross-sectional area of the nozzle ($d_j$=2 mm). In case 2, the PC pressure peak is delayed due to the less reactive initial mixture conditions compared to case 3 ($T_{in,2}$=300 K vs $T_{in,3}$=430 K). The main chamber ignition is also delayed for the same reason. In both cases, the initial hot jet exit does not show any OH*, indicating flame quenching within the nozzle or in the main chamber.

In case 2, the hot jet is first observed in the main chamber around 5.95 ms after spark, with the jet penetrating fast into the main chamber and impinging on the lower wall. Early penetration Schlieren images (e.g. at 6.3 ms) show very low signal near the jet tip, indicating low temperature gradients and thus strong mixing at that location. The fist OH* signal is observed at the jet core near the nozzle at about 9.65 ms, at the time that the pressure difference between the two chambers and thus the jet velocity fall to very low values. The OH* signal then completely disappears before significant signal is observed again at around 13 ms at different locations along the jet. Significant main chamber pressure increase indicating heat release and widespread OH* signal are only observed after 15 ms, resulting in a total ignition delay between hot jet exit and widespread ignition of ~9 ms.

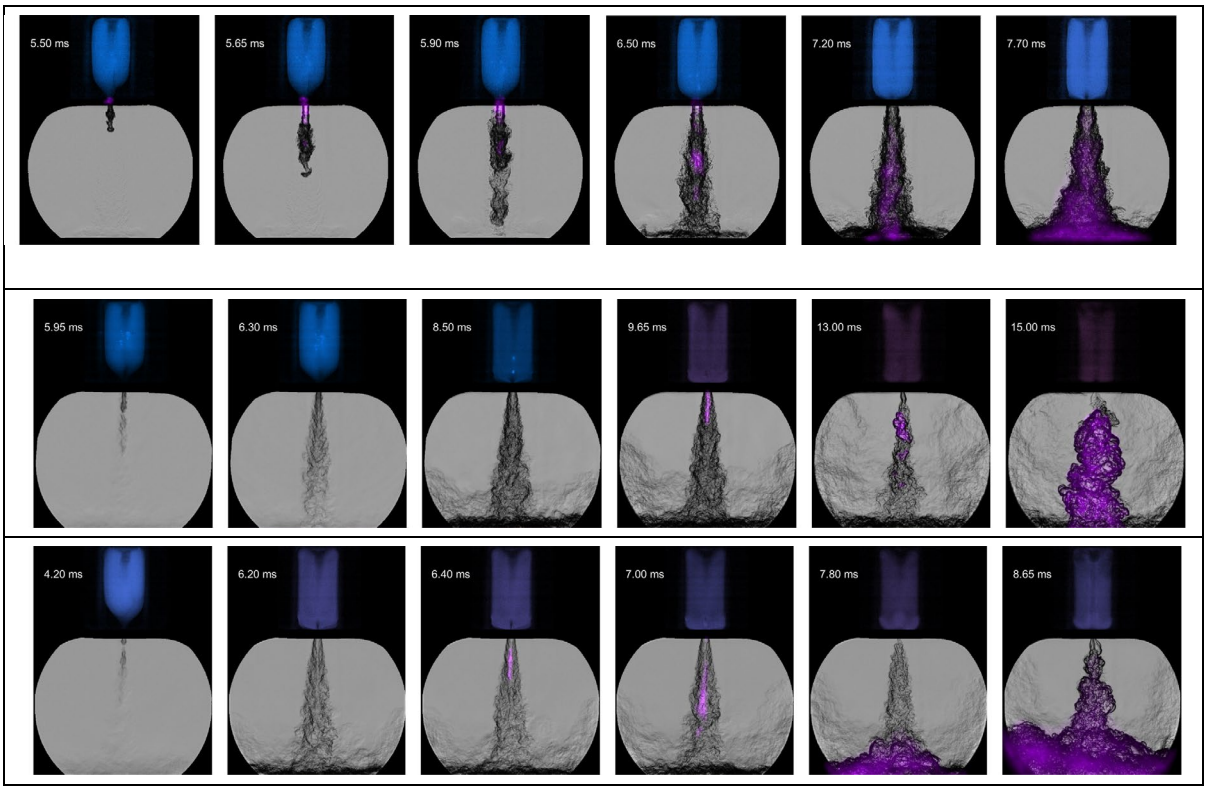


**Figure 8. Schlieren images of the main chamber with superimposed OH* (purple) for one repetition of the OPC case 1 (upper), 2 (middle) and 3 (lower series of images).**

The jet in case 3 shows a similar behavior to case 2, but with an accelerated sequence of events. The hot jet exit is observed at 4.2 ms, followed by the first OH* signal at 6.4 ms near the nozzle exit. The OH* area then expands and is finally convected towards the wall, before widespread ignition and main chamber pressure increase after 8.3 ms. The ignition delay time of ~4 ms in this case is shorter than in case 2.

Overall, it is observed that in case 1 there still exists a reaction zone at the nozzle exit, as indicated by the OH* signal, suggesting no complete quenching within the nozzle. The flame is nevertheless quenched downstream of the nozzle, when the hot products mix sufficiently with the cold unburned gases in the main chamber, suggesting quenching due to mixing. In cases 2 and 3 we observe complete quenching either in the nozzle or directly at its exit, while the pressure difference between the two chambers, and thus the jet velocity, is high. When the pressure difference decreases, we observe a reactive jet exiting the nozzle, which quenches downstream, again indicating quenching through mixing. Finally, despite similar phenomenology, case 3 re-ignites faster than case 2, highlighting the effect of initial temperature on the re-ignition propensity of the burned/unburned mixture created.

### 3.1.1 Flame quenching mechanisms

In order to understand the phenomena observed in the measurements, the experimental data is analyzed using simplified models. Quenching in a turbulent reacting jet passing through a nozzle into a chamber with unburned (cold) mixture can occur due to two distinct mechanisms (**Figure 9**). The first is thermal quenching, whereby the heat losses towards the nozzle wall exceed the heat release of the flame. The second mechanism, named hydrodynamic quenching, is caused by the intense mixing of the

combustion products emanating from the prechamber with the cold unburned mixture found in the main chamber.

Thermal quenching caused by wall heat losses may be relevant in turbulent jet ignition applications due to the large surface-to-volume ratio within the nozzle and the strong interaction with the nozzle walls during the passage of the flame. Wall quenching refers to the inability of a flame to sustain wall heat losses below a certain distance from the wall. Surface kinetics may also play a role when the wall is chemically active. The critical distance below which flame quenches ($\delta_q$) over the laminar flame thickness ($l_f$), is referred to as the Peclet number ($Pe$) and for side-wall quenching (i.e. during flame propagation parallel to the wall) it has a value [39]

$$Pe = \frac{\delta_q}{l_f} \approx 10$$

The equation above indicates that quenching will be more probable when the flame thickness is large (low chamber pressure) or the nozzle is very narrow.

Hydrodynamic quenching is the process whereby the flame quenches due to reduced temperature from mixing with the cold unburned gases. The propensity of quenching by mixing is characterized by the non-dimensional Damköhler number

$$Da = \frac{\tau_{mix}}{\tau_{fl}} = \frac{l_I/u'}{l_f/S_l}$$

comparing the relative timescale of the flame $\tau_{fl}$ to that of mixing $\tau_{mix}$. Due to the time- and space-varying nature of turbulence within the jet, the evaluation of a single Damköhler number is not straightforward for such a case. For the present investigation we choose to estimate $Da$ sufficiently downstream the nozzle exit (five nozzle diameters), where turbulence has already developed.

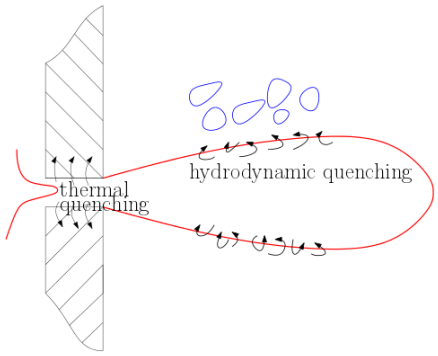


**Figure 9. Schematic of the different quenching mechanisms encountered in turbulent jet ignition applications.**

While the aforementioned criteria for flame quenching are indicative of the quenching propensity, they do not offer insights into whether the mixture will ignite – and if so, how fast – once quenched. This information would be important to judge whether quenching, if it occurs, can actually have a profound effect on the combustion of the MC charge, or whether it can be neglected. In cases where reactivity is very high and re-ignition is imminent, the assumption of no quenching might adequately depict reality, and can possibly be used in 3D CFD and quasi-dimensional simulations without introducing significant error. From this perspective, a simplified ignition delay time (IDT) for a homogeneous mixture consisting of unburned and burned gases can be computed, which can serve as a proxy for eventual ignition processes

$$\tau_{ign} = f(p, T_u, T_b)$$

This quantity can be calculated using a perfectly stirred reactor (PSR) with a mixture that is presumed to contain only the main combustion products ($CO_2$ and $H_2O$) and unburned gases. Having calculated the reactant temperature for the products of complete combustion, the PSR initial temperature is given as a function of unburned mixture fraction (ξ) assuming adiabatic mixing of the burned and unburned gases. This allows the calculation of the ignition delay for different ξ, which will tend to zero at ξ=1 (i.e. fully-burned products). This simplified approach neglects the effect of combustion radicals coming from the prechamber on main chamber ignition. These can only be taken into account using significantly more complex physicochemical modelling, which is performed in the numerical investigations of the project. A short ignition delay indicates that re-ignition is likely to occur under the given thermochemical conditions. In contrast, a mixture with long IDT will most likely not reignite.

### 3.1.2 Understanding of the experimentally observed phenomena

Using the analysis described above, we are able to compare the different cases measured in the OPC. The flame thickness for the different cases can be evaluated numerically, so that the quenching distances are

$$\delta_q \approx 10\, l_f \approx 0.4\, mm, \text{ for case 1 and 2}$$

and

$$\delta_q \approx 10\, l_f \approx 0.35\, mm, \text{ for case 3}$$

In all cases the quenching distance is much shorter than the nozzle diameter ($d_j$=4 mm in case 1 and 2 mm in cases 2 and 3). This means that based in this simplistic approach, thermal quenching is not expected under the considered thermochemical conditions.

We can also use the same methodology to evaluate the evolution of the Damköhler number in time for a fixed jet position (five nozzle-diameters downstream nozzle exit). **Figure 10** shows the evolution of the mixing state (blue, solid) and the flame reactivity (blue, dashed) timescales, as well as the resulting flame Damköhler number (red). In all cases the mixing timescale and thus the resulting Da starts from low values and then increases due to a reduction of the jet velocity, and thus turbulent intensity. For the larger nozzle in case 1, the initial Da is higher than in the other two cases ($Da_1$=0.5, $Da_2$=0.075, $Da_3$=0.1), indicating lower quenching propensity. The lower Da in case 2 compared to case 3 is due to the lower mixture reactivity, as a result of the lower temperature. Interestingly, in cases 2 and 3 the experiments show appearance of the OH* signal when the Da reaches a value of ~0.15. In all, the combination of the analysis using the 0D model and the experiments indicate that at Da~0.5 the flame downstream of the nozzle is quenched, which means that a subsequent re-ignition is necessary.

In order to study the re-ignition process, perfectly stirred reactor calculations for various burned/unburned mixture compositions were used. **Figure 11**(a) shows the combined effect of mixing (movement towards lower mixture fractions) and mixture reactivity (unburned gas temperature). In case 1, lower mixing rates are expected to result in higher mixture fractions, resulting in shorter ignition delays, as observed. In cases 2 and 3, similar mixing is observed, but the difference in the ignition delay (~9 vs ~4 ms after jet exit) is the result of the nearly half-order of magnitude difference in ignition delay at a constant mixture fraction. **Figure 11** also includes the ignition delay for the case of lean composition in the prechamber ($\varphi_{MC}$=$\varphi_{MC}$=0.75), showing the effect of differences in the temperature of the prechamber products on ignition.

The same analysis can also be performed for engine applications to estimate the propensity for flame quenching due to thermal losses or mixing, and for re-ignition when quenching is present. Using a tuned 0-D engine model for the Liebherr engine, the parameters relevant for thermal and mixing-induced quenching were calculated, and are included in **Table 3**. The operating conditions chosen were a

reference condition at high load, a condition where a prechamber with higher nozzle area ($A_{noz}$) to prechamber volume ($V_{pc}$) ratio was used, and a point at low load operation.

The engine results show smaller flame thicknesses compared to the OPC, as expected from the significantly higher pressure. This results in low tendency to quench due to thermal losses in the nozzle, since the resulting quenching distance is significantly lower than the nozzle dimension. In fact, for most engine applications the pressure at ignition is expected to be significantly above the conditions accessible in the OPC, which means that barring very small prechamber nozzles, thermal quenching should not be expected. At lower loads the tendency for thermal quenching will increase, but it is expected to not be important.

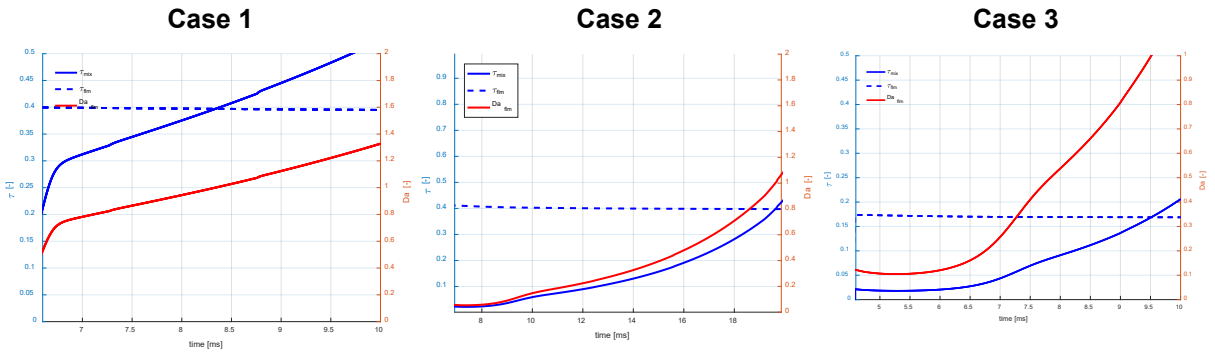


**Figure 10. Evolution of mixing (blue, solid) and flame reactivity (blue, dashed) timescales, and the resulting flame Damköhler number (red) for the three OPC cases.**

In terms of the calculated flame Damköhler number, in all cases considered here the values are similar to the OPC. As expected, with higher $A_{noz}/V_{pc}$, the Da reduces, due to reduced jet velocity and resulting mixing. At low loads the Da also reduces slightly, as a result of slightly lower mixing due to lower pressure difference over the nozzle. In all, the Da values observed, when compared to the values from the OPC, indicate that even for this unscanvenged prechamber application flame quenching due to mixing could be expected. Considering the higher jet velocities observed from scavenged prechambers, it seems plausible to also expect high quenching tendencies due to mixing in the jet exit in such applications. With reduced load, the quenching tendency is expected to drop, but only slightly as was observed in this study.

**Table 3: Operating conditions and quenching parameter results for a typical unscavenged prechamber lean-burn engine**

| Operating condition | $P_{sp}$ | $T_u$ | $\lambda$ | $l_f$ | $\delta_q$ | $\tau_{mix}$ | $\tau_{fl}$ | $Da_{fl}$ |
|---|---|---|---|---|---|---|---|---|
| | bar | K | | mm | mm | ms | ms | |
| Reference | 76 | 814 | 1.7 | 0.016 | 0.16 | 0.032 | 0.16 | 0.2 |
| High $A_{noz}/V_{pc}$ | 63 | 813 | 1.7 | 0.016 | 0.16 | 0.075 | 0.15 | 0.5 |
| Low load | 38 | 810 | 1.7 | 0.023 | 0.23 | 0.036 | 0.16 | 0.225 |

Considering that flame quenching is expected, it is interesting to study the expected ignition delay (ID). **Figure 11** shows the calculated ignition delays for different charge pressures, for a constant composition of equal burned and unburned gas mass fractions (ξ=0.5). The different lines correspond to the reference conditions (blue, solid – T=800K, λ=1.7), different unburned gas temperatures (magenta, dotted/dashed: T=600K, λ=1.7; green, dashed: T=700K, λ=1.7), and different charge composition (red, dotted: T=700K, λ=1.0). The variation in pressure was chosen since this will be the major change when varying the engine load (low load: lower pressure). The changes in unburned temperature represent engine designs with lower compression ratio, or cold starts. The case with stoichiometric operation was chosen as representative for automotive/mobile applications using a 3-way catalyst.

The results show that the times for re-ignition are significantly shorter than observed for the OPC, as expected due to the higher temperature and pressure in the engine application. For the conditions encountered in the Liebherr engine at full load, ID for this mixture fraction is expected to be around 0.2 ms, which can be assumed to be negligible for any application, especially since the time needed to reach this level of mixing will probably be longer. Even for very low loads (10 bar, throttled operation), the ignition delay rises to around 1 ms, which is still very short compared to the OPC. This indicates that even if quenching takes place in such an engine application, the re-ignition will be fast enough for quenching not to be observable.

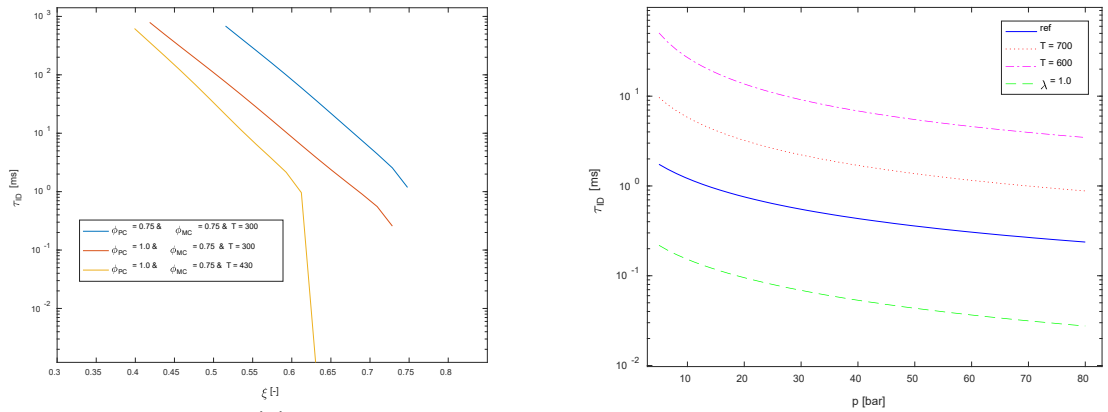


(a) (b)

**Figure 11. (a) Effect of mixing and mixture reactivity on ignition delay time; (b) Ignition delay calculated using perfectly stirred reactors with equal burned/unburned mass fractions (ξ=0.5), for different mixture compositions and unburned gas temperatures. Reference T=800K, φ=0.6.**

With lower charge temperatures (700 K and 600 K), the ignition delay increases significantly. This means that for engines with low compression ratios, quenching of the PC flame is expected to be more apparent. In addition, during cold start, engines with prechambers might have difficulties to ignite the main chamber mixture, depending on whether quenching is experienced and sufficient temperature and pressure builds up during compression. This can provide a guideline for prechamber design, to allow engine cold-start and a wide operating range. For the stoichiometric engine application (prevalent in on-road applications), the observed ignition delay is significantly shorter, signifying possibly reduced effect of flame quenching for such engines.

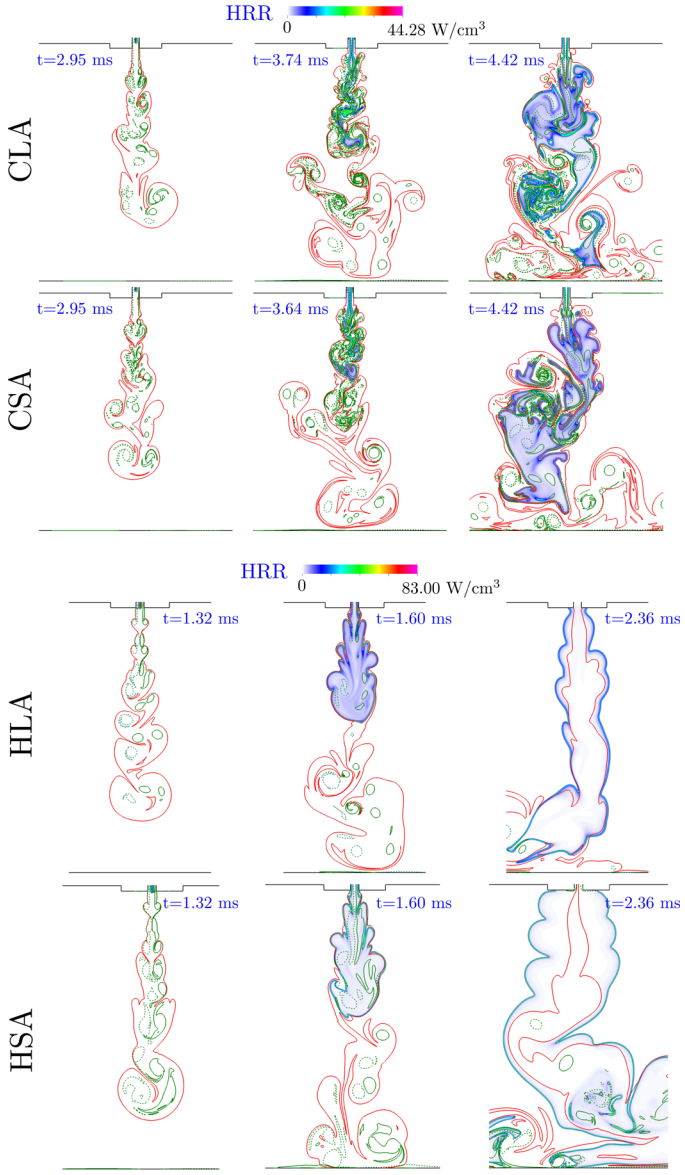


**Figure 12. Instantaneous isolines of vorticity (dashed and solid green lines for negative and positive vorticity), mixture fraction ξ= 0.1 (red line) and distribution of HRR in the main chamber for the dj=1.5 mm nozzle in cases CLA: $T_u$=300 K, $\varphi_{MC}$=0.5, adiabatic walls, CSA: $T_u$=300 K, $\varphi_{MC}$=1.0, adiabatic walls, HLA: $T_u$=800 K, $\varphi_{MC}$=0.5, adiabatic walls, HSA: $T_u$=800 K, $\varphi_{MC}$=1.0, adiabatic walls.**

## 3.2 Numerical investigations

### 3.2.1 Two-dimensional DNS

The parametric 2-D simulations of turbulent jet ignition of premixed methane/air mixtures in the pre- (PC) and main chamber (MC) assembly provided a detailed description of the ignition and combustion phenomenology under different initial flow (quiescent and turbulent flow) and thermochemical (low and high initial temperature for lean as well as stoichiometric main chamber mixture) conditions, wall thermal boundary conditions (isothermal or adiabatic), geometric characteristics (nozzle diameter with smooth and sharp entry) and spark location.

Three phases can be discerned. During the first phase, the combustion in the PC that is initiated by a hot kernel generates a transient non-reactive stoichiometric jet in the MC, which in turn generates strong turbulence in the region close to the nozzle exit as well as a close to stoichiometric mixture in the main chamber, irrespective of its initial composition. During the second phase, a hot reactive jet exits into the MC to initiate ignition and form the flame that consumes the MC mixture. During the final phase, the pressure increase in the MC results in flow reversal from the main to the prechamber.

The effects of the initial temperature and equivalence ratio in the main chamber on combustion phenomenology are presented in a paper submitted to Combustion and Flame, while a second publication discussing the effects of nozzle shape and width, initial turbulence and spark location is in preparation. **Figure 12** shows instantaneous isolines of vorticity (dashed and solid green lines for negative and positive vorticity), and mixture fraction $\xi$= 0.1 (red line) superimposed on the distribution of HRR in the main chamber for the narrow width ($w_j$=1.5 mm) nozzle. The vorticity isolines are indicative of the flow structures generated by the prechamber jet, while $\xi$=0.1 approximately marks the region where the PC fluid has reached. In the lean MC cases, it further defines the area where the composition is stratified.The time instants were chosen as the time that the hot jet is about to exit the orifice (left column), prior to jet impingement on the lower wall (middle column), and shortly after the flame exits the part of the domain shown (right column).

The initial temperature has a strong effect on flame propagation in the PC, while the effect of the wall thermal boundary conditions is minor, enhancing only slightly the rate of flame growth when the isothermal wall is hotter that the unburned mixture. During propagation, the flame in the PC is thicker than the 1-D unstrained premixed flame in all cases. As the flame front approaches the walls, the heat release rate increases for the cases of positive wall heat flux or adiabatic wall. It was observed, however, that the maximum temperature of the burnt gases exiting the PC decrease significantly below the corresponding adiabatic flame temperature, particularly for the narrow nozzles where the decrease in temperature ranges between 300 and 585 K in the $T_u$=800 K and 300 K, respectively. The decrease of the mean temperature at the nozzle exit can be even higher and persists during the whole period. This indicates that the prechamber design plays an important role in the heat loss from the flame so that the heat released can be more effectively used to ignite the MC mixture.

Furthermore, despite the short residence time in the nozzle, reactivity is globally (i.e. with respect to the mean progress variable) enhanced in the $T_u$=800 K and reduced in the $T_u$=300 K cases. The effect on the radicals depends on the species kinetics. For example, the mean mass flux of OH shows a similar trend as the progress variable, while $HO_2$ formation is favored by the reduction in temperature. The wall thermal boundary condition was found to have only a minor effect on reactivity in the orifice because of the short residence time.

The unburned mixture temperature plays a dominant role in the size and intensity of the vortical structures generated in the main chamber by the non-reactive jet of the first phase: small and strong vortices are formed and persist in the cold case, while the weaker vortices dissipate quickly in the hot, higher viscosity cases. This has a pronounced effect on the hot reactive jet that subsequently exits the PC. In the $T_u$=300 K case (**Figure 12**, cases CLA and CSA), the jet is broken into small kernels, which, however, can remain trapped inside the fully-burned mixture, and thus become ineffective for ignition of the MC charge. At the same time the intense vorticity creates a larger interface, enhancing mixing with the MC gases. In combination with its slow propagation speed, the flame front remains highly convoluted until eventually a propagating front is formed. The local flame structure differs significantly from that of

a laminar premixed flame, and turbulent combustion models that can this into account should be used for modeling.

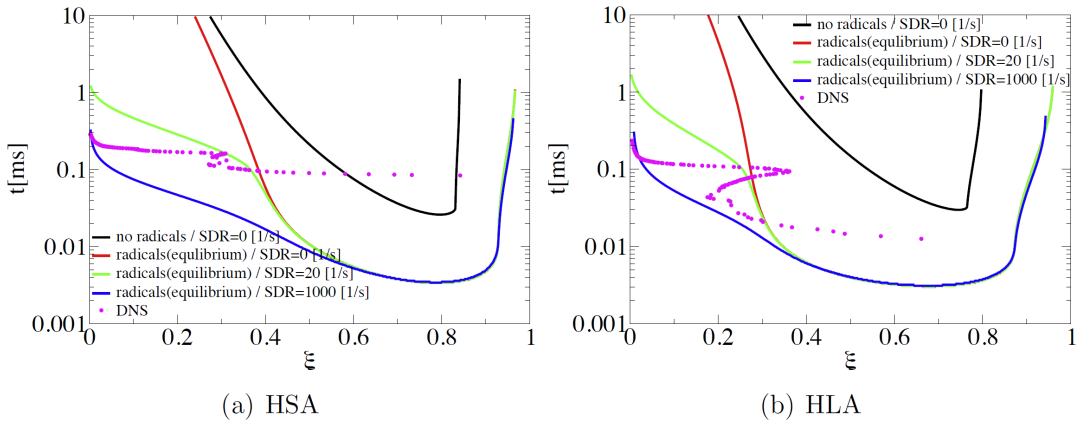


**Figure 13. Comparison of the ignition delay time predicted using a conditional moment closure model with different values of scalar dissipation rate (SDR) and composition of the fully-burned mixture with the results extracted from the 2-D DNS. Hot mixture ($T_u$=800 K) with (a) φ=1 and (b) φ=0.5.**

In the $T_u$=800 K case, a flame torch with a relatively smooth front is created close to the nozzle exit (**Figure 12** cases HLA and HSA). When the MC mixture is stoichiometric, the flame propagates in the normal to the jet direction while the torch is convected towards the lower wall by the jet. A similar behavior is observed in the lean case, albeit with a slower propagation in the lateral direction. The torch impinges on the lower wall, creating large vortical structures which enhance the flame growth rate and consequently the fuel consumption. The local flame structure becomes similar to that of the 1- D premixed flame in the $\varphi_{MC}$=1 case, or is bounded by that of the stoichiometric and the lean 1-D flame in the case of the lean main chamber mixture. The similarity is attributed to the fact that due to higher reactivity the established flame front escapes faster from the regions where the PC burned gases can affect the flame. The energy supplied by the PC burned gases to the MC flame front leads to superadiabatic temperatures, and this is more pronounced in the cold cases where the flame front remains trapped in the regions of the intense flow field generated by the jet from the prechamber. Jet impingement on the lower wall also plays an important role by creating large-scale vortices, which bring fresh fuel in contact with the hot jet and the propagating flame to enhance consumption of the MC mixture.

The effects of nozzle geometry (width and smoothed vs. sharp entry), initial flow in both chamber (quiescent vs. turbulent), and spark location for different initial temperatures and MC compositions are discussed in a paper under preparation. Sharp corners at the nozzle inlet result in the generation of more more intense turbulence in the main chamber by the non-reactive jet. For a lean MC mixture, there is significant enhancement of the heat release rate (HRR) at the orifice exit. At the same time, the hot jet penetrates less in the MC as it is deflected by the turbulent flow. For stoichiometric main chamber conditions, the enhancement in HRR for sharp corners is less pronounced. Shorter penetration also reduces the influence of the lower wall on the increase of flame area, resulting in lower rate of heat release. Similar effects are observed in the cases where the flow is initialized with decaying turbulence.

The effect of spark location was studied for two cases of large nozzle width, where the influence of the lower wall is less important. When the spark is located close to the upper PC wall, the longer combustion duration results in a jet with higher velocity, and thus leads to deeper penetration and generation of more intense turbulence in the main chamber. Overall, a higher heat release rate is observed which is slightly delayed with respect to what is observed when the spark is located at the center of the

prechamber. In the latter case, a smooth flame torch is established at the orifice exit and a smooth flame front propagates to consume the fuel in the main chamber.

Turbulent jet ignition can be characterized by two times. The first is determined by the ignition of the most reactive mixture fraction while the second is the time of ignition of all mixing states that have been created by mixing of prechamber gases with the main chamber mixture. Flamelet simulations were performed to study the effect of scalar dissipation rate (SDR) and the presence of radicals on both times (**Figure 13**). It was found that at the considered conditions the presence of radicals in the hot reactive jet decreases significantly the ignition delay time (IDT) of the most reactive mixture fraction and create an extended plateau of mixtures with short IDT (colored lines) in comparison to the case where the PC mixture is burned fully to $CO_2$ and $H_2O$ (black lines). The assumption of complete consumption may only be relevant at the high pressures that exist in internal combustion engines, which suppresses dissociation reactions. It was also found that the scalar dissipation rate does not affect significantly the most reactive mixture fraction and the corresponding ignition delay time. However, increasing SDR results in significant reduction of the time needed to ignite mixtures away from the most reactive condition. While the most reactive mixture fraction is predicted well by the flamelet calculations, the ignition delay time in the 2-D simulations is significantly longer (purple points). Extinction and reignition of different mixing states were also observed in the 2-D simulations, as can be seen by the existence of multiple ingnition times for $\xi$~0.2 – 0.3.

## 3.3 Three-dimensional DNS

### 3.3.1 Simplified setup

The two main chambers compositions considered with equivalence ratio of either $\varphi_{MC}$=0.5 or $\varphi_{MC}$=0.75 resulted in either gradual or fast fuel consumption in the main chamber (**Figure 14**), similar to what has been observed experimentally and in the lean 2D cases. The Reynolds number at the inflow is initially $Re_0$=5938 and increases to twice this value when the maximum inlet velocity is ramped up as shown in **Figure 6**(b) and (c). The computational cost for these cases is indicative of the cost for the full geometry and varies from 3.9 and 5 million CPUhr in the $\varphi_{MC}$=0.5 and $\varphi_{MC}$=0.75 case, respectively.

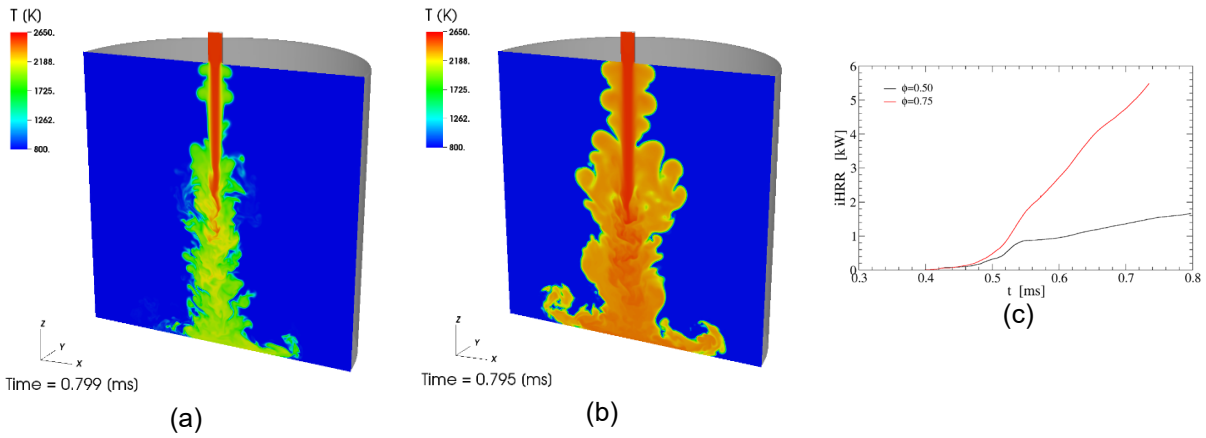


**Figure 14. (a), (b) Distributions of temperature on a plane through the domain axis for the $\varphi_{MC}$=0.5 and 0.75, respectively); (c) temporal evolution of the integral of the heat release rate in the entire domain.**

Distributions of different quantities obtained by post-processing of the raw data at two time instants are shown on vertical slices through the domain axis in **Figure 15**. The quantities shown from left to right are the heat release rate, progress variable based on the mass fraction of oxygen, mixture fraction,

vorticity superimposed with the flame front location, and mass fraction of the hydroxyl radical. As indicated by the strong vorticity about 3 nozzle diameters away from the orifice exit, the breakup of the non-reactive jet generated intense turbulence in part of the initially quiescent flow. At t=0.44 ms, shortly after the injection of hot reactive jet, the reactive jet has just reached the top of the region with high turbulence intensity, as can be more clearly seen in the vorticity plot. Only 0.1 ms later (bottom figure) the flame at the domain center is strongly convoluted and broken by turbulence into a multitude of reaction zones. At the same time, the torch flame close to the nozzle exit has the typical structure of a premixed flame.

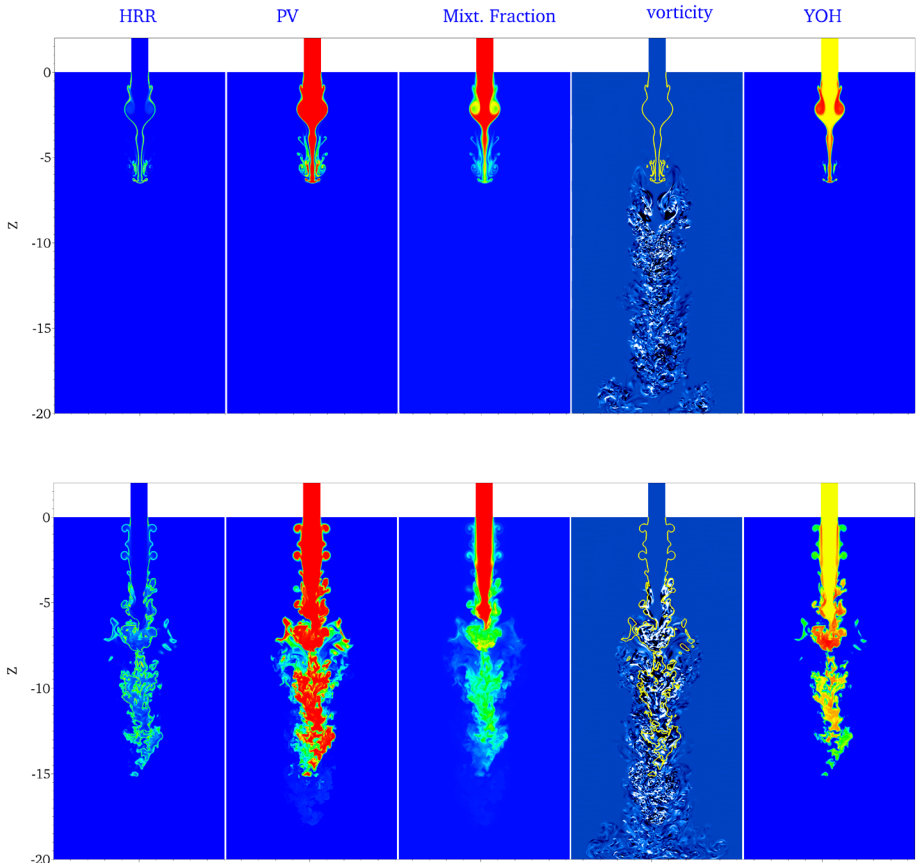


**Figure 15. Distribution of heat release rate, progress variable, mixture fraction, vorticity superimposed with the flame front, and OH mass fraction (from left to right) at t=0.44 ms (top) and 0.54 ms (bottom).**

The simulations reveal that depending on the unburned mixture reactivity (determined by $\varphi_{MC}$) and the local flow and mixing conditions, different combustion modes coexist in the main chamber. A propagating flame is established close to the nozzle exit in the $\varphi_{PC}$=0.75 case, while the hot reactive mixture in the leaner case could not initiate a propagating front during the simulated period. Between 5 and 10 mm away from the nozzle exit, the local turbulence that generated during the first 0.4 ms of the injection of the non-reactive results in strong mixing with the colder surrounding fluid. When the burning mixture enters this region, the flame initially extinguishes but establishes favorable local conditions which become more prone to ignition by the hot reactive gases that are supplied at the inflow. In the $\varphi_{PC}$=0.75 case, ignition is also observed close to the lower wall by the partially reacted mixture convected from upstream, as can be observed in the volume rendered instantaneous distributions of OH mass fractions within the domain for both case shown in **Figure 16**.

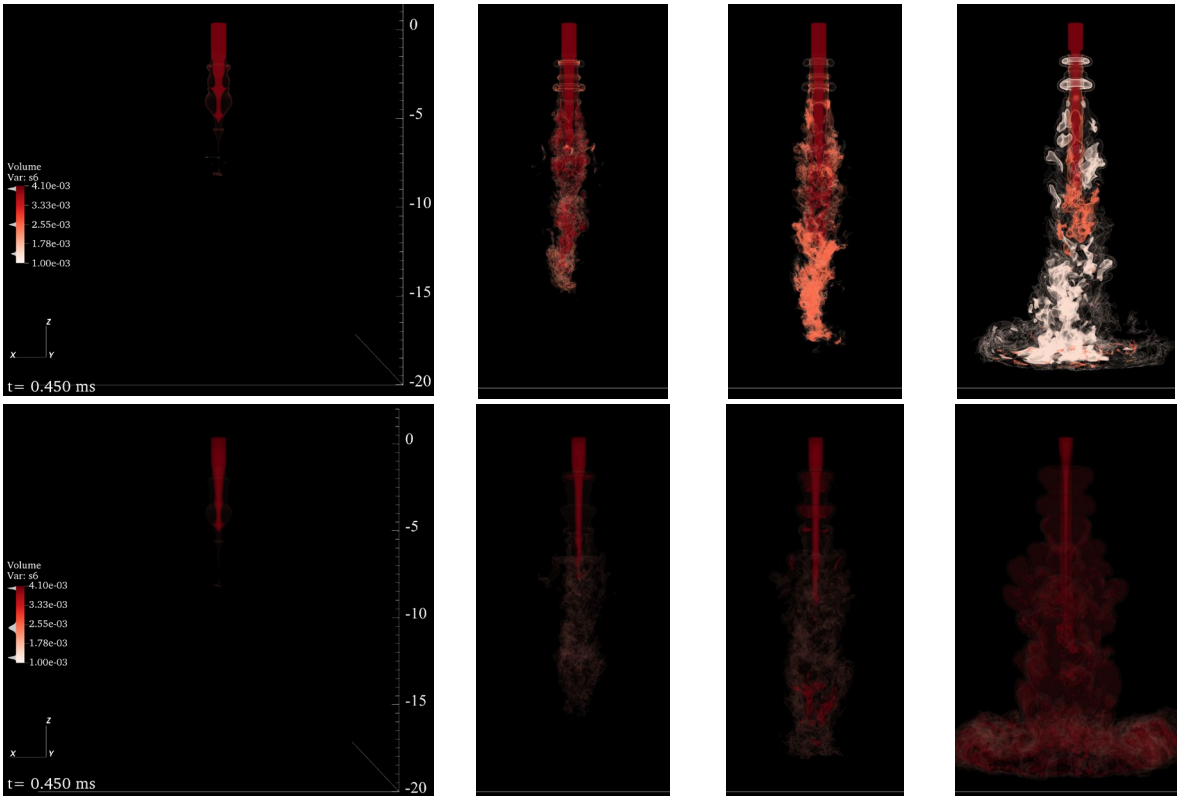


**Figure 16. Volume renderings of OH mass fraction in the simplified setup for $\varphi_{PC}$=0.50 (top) and $\varphi_{PC}$=0.50 (bottom) and t=0.45, 0.55, 0.60 and 0.80 ms (from left to right).**

Post processing of the raw data is underway, aiming to (a) study the phenomenology and compare it to that of the 2D cases, (b) study the effect of dimensionality on the local flow, mixing and flame structure/combustion mode, and (d) provide data for LES, which are obtained with well-defined initial and boundary conditions and without the uncertainties associated with the difficulty of accurately accounting for the intense flame/wall interaction during flame propagation in the PC. The observed complex phenomenology has implications for modeling, since the combustion model should account for both combustion modes.

### 3.3.2 Pre- and main chamber assembly

The simulation was performed using a computational mesh with 973,552 spectral elements locally refined around the walls and within a cone that contains the evolving jet. Polynomial orders ranging between N=7 and 11 were used in order to capture the evolution and the small-scale structures generated during penetration of the jet in the main chamber, resulting in approximately 335 million to 1.3 billion unique grid points. The total computational time was 11.4 million CPUhr for the simulation of 4.3 ms of the process. The post-processing of the close to 11.5 TB of the generated raw data is underway and will continue after the project completion

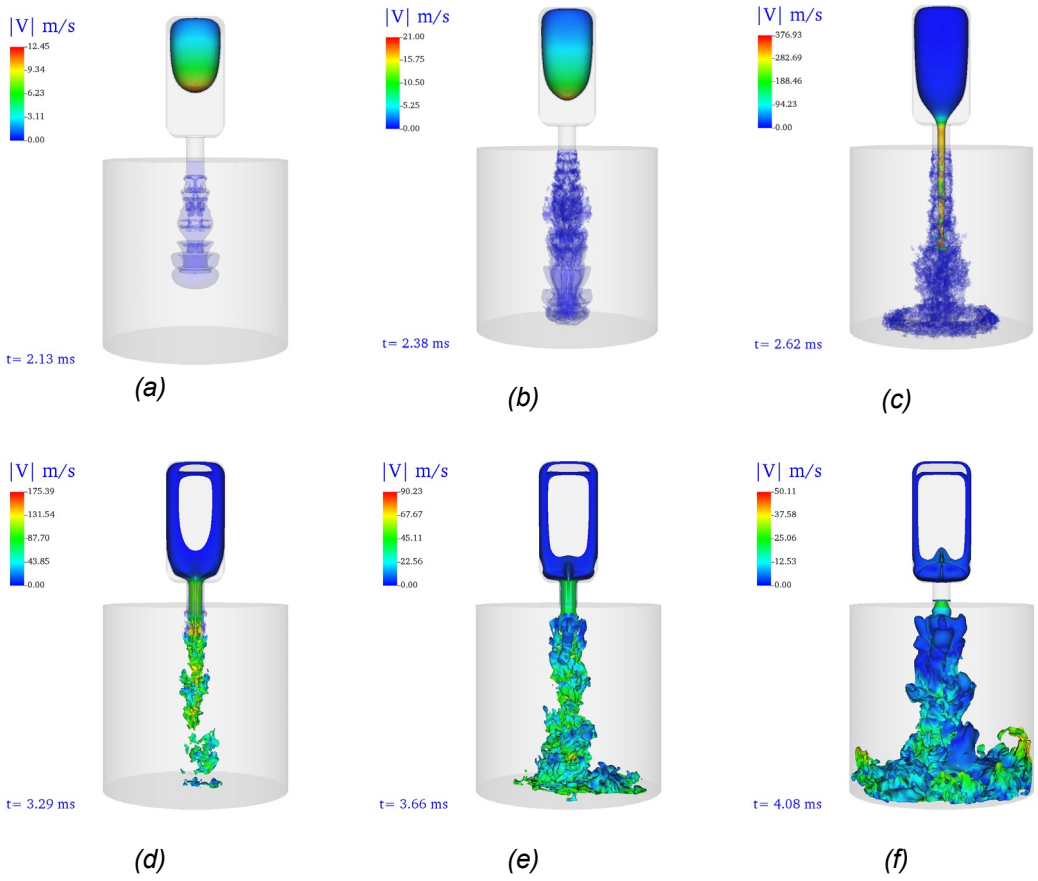


**Figure 17. (a)-(f) $Y_{CH4}$=6.7e-3 isosurfaces marking the flame front colored by the velocity magnitude. In (a)-(c) superimposed is the isocontour of φ=0.9 in the main chamber.**

The geometry and dimensions of the computational domain was presented in **Figure 6**(c) as well as the evolution of the $Y_{CH4}$=6.7e-3 isosurface which was found to follow well the location of maximum rate of heat release colored by the velocity magnitude. In **Figure 17**(a)-(c) in blue is the φ=0.9 isosurface resulting from the local enrichment of the main chamber gas by the stoichiometric mixture ejected from the prechamber. The bottom figures show that the flame has consumed a significant fraction of the MC charge, while in **Figure 17**(f) the fuel in the prechamber is almost totally consumed and the flow in the orifice has changed direction due to the pressure increase in the main chamber pushing main chamber mixture into the prechamber. Analysis of the very dataset generated by the DNS is currently underway and will also continue after project completion.

## 3.4 Reynolds Averaged Navier-Stokes and Large Eddy Simulations

In order to build computationally efficient models to support the already performed as well as future experimental investigations, we extended beyond what was originally proposed towards the development of Reynolds Averaged Navier-Stokes and Large Eddy Simulation models using a commercial code. RANS was performed using the RNG k-ε turbulence model and the SAGE chemical kinetics using the GRI-3.0 reaction mechanism. The second order CDS scheme was used for spatial discretization and the considered experimental conditions are summarized in **Table 4**. The peak cell

count was 3.75 million cells and the computational wall-clock time was about 55 hours on 48 cores for the simulation of 50 ms.

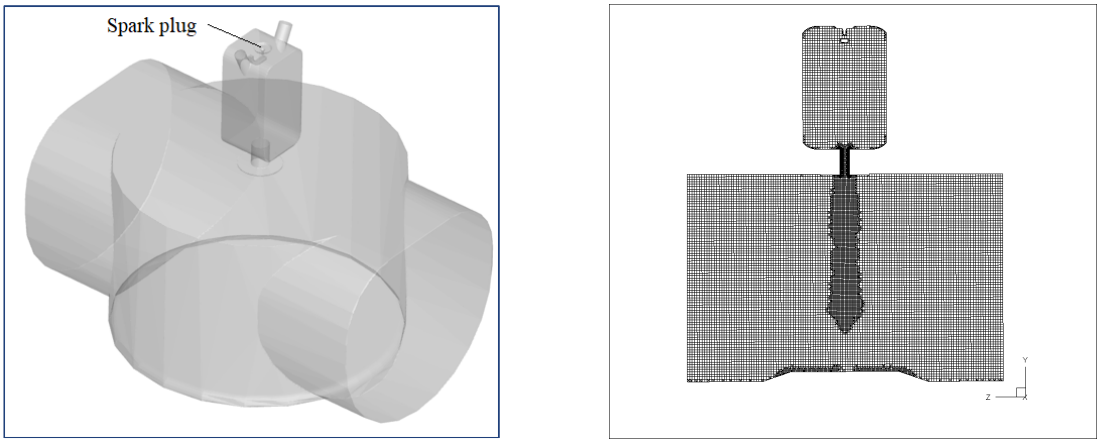


**Figure 18. (a) Computational domain used in the RANS and LES, (b) an example of adaptive local mesh refinement generated by CONVERGE CFD.**

As can be seen in the comparison of the experimental and computed pressure profiles shown in **Figure 18**, the computed time history of pressure is in good agreement with the measured. Despite the higher resolution, the LES appears to be more sensitive to modeling details, and up till now the profiles could only be captured qualitatively, while the location of the peak pressures in the pre- and main chamber appear later than in the experiments. We will employ higher resolutions and explore the performance of different turbulence and combustion models.

**Table 4. Selected experimental cases used for RANS.**

| Case | Nozzle diameter (mm) | Initial pressure (bar) | Initial temperature (K) | Equivalence ration Main chamber (-) | Equivalence ration Pre-chamber (-) |
|---|---|---|---|---|---|
| 1 | 2 | 5 | 450 | 0.75 | 1.0 |
| 2 | 2 | 5 | 300 | 0.75 | 1.0 |
| 3 | 2 | 5 | 450 | 0.6 | 1.0 |
| 4 | 4 | 1 | 450 | 1.0 | 1.0 |
| 5 | 4 | 5 | 300 | 0.75 | 1.0 |

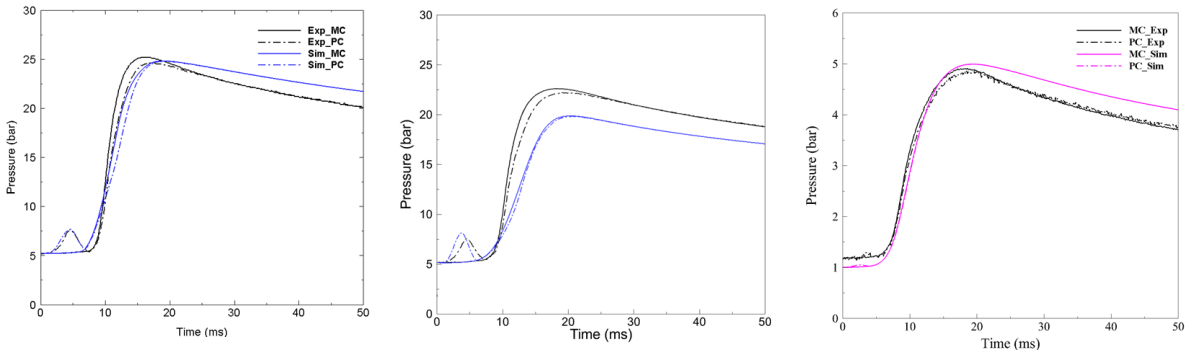


**Figure 19. Comparison of experimental and RANS pressure traces for cases 1, 3 and 4 (from left to right).**

# 4 Conclusions

Prechamber ignition systems exploit the hot turbulent jets generated by combustion in a small prechamber (PC) attached to the main chamber (MC) of the combustion device, in order to ignite and sustain the consumption of difficult to ignite mixtures. The whole process is characterized by different sub processes, including spark ignition of the typically richer prechamber mixture and flame propagation within the small prechamber, a gradually developing transient flow of the unreacted PC mixture that generates intense turbulence close the exit of the orifice connecting the two chambers, flame propagation though narrow nozzles and into the turbulent conditions generated by the preceding non-reacting jet, ignition of the MC fluid, and establishment of a propagating flame to consume the charge. All these processes interact with each other, and are sensitively affected by the geometry of the two chambers and of the nozzle, the spark location in the PC and the initial flow and thermochemical state. It is thus not surprising that they lead to a complex phenomenology that is difficult to capture, understand and model.

A combination of different approaches was used to address the challenges. An optically accessible pre- and main chamber assembly was designed, constructed and employed to investigate flame propagation in the prechamber as well as ignition and fuel consumption in the main chamber. Pressure was recorded in both chambers together with high-speed images of Schlieren and OH* chemiluminescence, and the setup was equipped with sensors to measure wall heat fluxes. The state-of-the art facility allows for separate filling of the two chambers with mixtures of different composition, and is automated to repeat each measurement multiple times in order to assess repeatability. The OH* chemiluminescence signals indicated that the hot turbulent jet can be partially quenched either as it passes through the nozzles, or hydrodynamically by the intense mixing with the cold gas in the main chamber, and an attempt was made to characterize the observed behavior and extract general criteria that can be used for engine operating conditions using the recorded information and low-order models.

A more complete description of the system with high temporal and spatial resolution was obtained using direct numerical simulations (DNS) with a skeletal reaction mechanism containing 20 chemical species. A computationally less intensive two-dimensional geometry was used to perform parametric DNS in order to investigate different aspects of the aforementioned processes at atmospheric pressure. Their strong coupling and their effect on the mode of combustion was clearly demonstrated. The latter was found to vary in space and time, and included localized ignition, flame propagation and breakup of the flame fronts into distributed reaction zones. It was also shown the flame is strongly affected as it propagates in the prechamber and its temperature and reactivity can be significantly lower than that of the laminar premixed flame. Despite the reduction in the concentration of the hydroxyl radical (OH), there was no indication of flame quenching. Numerical investigations focusing only on the effect of nozzle size on freely and forced propagating flames have been initiated to study the critical conditions (nozzle diameter and inflow velocity) for quenching. It was also shown that it is not accurate to consider

the PC mixtures as fully burned and that low-order modeling must take into account the production of minor species and radicals.

Three-dimensional DNS were performed in two setups. The first used a geometry where the PC was removed and its effect was modeled using time-varying boundary conditions at the inflow. This geometry simplification allowed for the consideration of higher pressure and provided better control of the conditions in the main chamber. The second setup is that of the experimental OPC, albeit with a smaller diameter MC cylinder. The raw data from both setups are currently post-processed and will be compared with the 2-D DNS and the experiments.

In order to model the experiments in a computationally efficient way, RANS and LES models have been constructed using a commercial code. Good agreement with the measured pressure signals could be obtained with the RANS model, while the LES needs to be further refined with respect to resolution and choice of turbulence and combustion models based on the findings from the DNS. In combination with quasi-dimensional models that have been developed at LAV in the frame of related projects, it is expected that the RANS and LES models will complement existing and future experimental campaigns and aid in their interpretation.

# 5 Outlook and next steps

The experiments and simulations have provided deep insights into the complex interactions of the multitude of processes governing prechamber ignition and generated rich datasets that could only be partially analyzed during the project duration. The on-going analysis of the data will continue after the completion of the project and the results will be presented in publications in peer-reviewed journals. A number of issues of fundamental as well as practical interest have also been pointed out by the combined experimental and numerical work, including the effect of the nozzle on the reactive state of the jet exiting into the main chamber and of the partial oxidation of the prechamber mixture, which we have started to study using direct numerical simulations. The RANS and LES models of the optical prechamber that have been constructed will be fine-tuned, and used to complement the experimental campaigns that have already been performed as well as the ones planned in the state-of-the-art OPC. Experiments and simulations are also guiding the development and provide validation data for the computationally efficient quasi-dimensional models built at LAV.

# 6 National and international cooperation

Two other projects in which the Aerothermochemistry and Combustion System Laboratory is involved in are related to this project: (i) collaboration with Liebherr Machines Bulle in the framework of a nationally funded KTI/CTI project and (ii) part of a much larger EU Horizon 2020 project (detailed in international cooperation).

The focus of the KTI/CTI project is on unscavenged prechamber combustion for natural gas engines in the heavy-duty range designed for power generation. The setup of the optically-accessible prechamber test rig and the design of the control system were performed in collaboration with the Institute of Thermal and Fluid Engineering of the University of Applied Sciences and Arts Northwestern Switzerland (FHNW) (Prof. Kai Herrmann and Dr. Alexey Denisov). The test rig will also be used within the project “Investigation of heat transfer (resolved in space and time) by modern combustion processes” (PI Kai Herrmann), which provides complementary experimental techniques for the understanding of heat transfer effects within the prechamber and in the lower main chamber walls.

The EU Horizon 2020 project 'GasOn' concentrated on the development of technologies and engine prototypes which use exclusively compressed natural gas (CNG). As opposed to current dual-fuel (gasoline and CNG) engines, the newly developed monovalent engine prototypes will have significantly higher efficiencies. Overall, a reduction in $CO_2$ emissions of the order of 20-25% compared to the gasoline equivalent engines is expected. GasOn WP5, in which LAV is one of the collaborators, is headed by Volkswagen AG. WP5 focuses on lean burn natural gas combustion using prechambers for passenger car size engines. The collaboration has provided valuable insights into the conditions of relevance for the engine applications, and has highlighted the importance of heat transfer from the prechamber jets on the opposing wall/piston surface.

# 7 Communication

We have recently initiated discussions with a group of U.S. national research laboratories consisting of Sandia, NREL, ANL and ORNL that perform experimental and modeling work on prechamber ignition systems. It is planned to continue collaboration towards the common goal of in-depth understanding of the complex phenomenology and its implications for modeling.

Parts of the work have also been presented in national and international meetings and conferences as listed below.

S. Benekos, G. Giannakopoulos, C. Frouzakis, K. Boulouchos, An exploratory parametric 2-D DNS study of prechamber ignition, 17th International Conference on Numerical Combustion, Aachen, May 6-8 2019

C.E. Frouzakis, G.K. Giannakopoulos, S. Benekos, M. Jafargholi, K. Boulouchos, DNS and LES of gas engine phenomena, 41st TLM IEA, Montreux, Nov. 3-8, 2019

G. Giannakopoulos, C.E. Frouzakis, K. Boulouchos, Extreme scale computing in combustion: contributions to physical understanding, theory and modelling, Conference on Combustion Research in Switzerland, Zurich, 24 June 2019

C.E. Frouzakis, CFD across scales for internal combustion engines and engine-related phenomena, Laboratory of Fluid Dynamics & Technical Flows, U. Magdeburg, June 11, 2019

C.E. Frouzakis, S. Benekos, G.K. Giannakopoulos, Direct numerical simulation of prechamber ignition, 40th Task Leader Meeting of Combustion, 2017, Frejus, France

M. Bolla, Towards understanding prechamber combustion, Second International Energy Agency / ERCOFTAC joint workshop on "Gas engine combustion fundamentals", ETH Zurich, June 18, 2018

M. Bolla, P. Kyrtatos, S. Benekos, K. Bardis, G. Xu, M. Kotzagianni, Y.M. Wright, G. Giannakopoulos, C.E. Frouzakis, K. Boulouchos, Pre-chamber ignition for lean-burn gas engines: A hierarchical approach to pre-chamber combustion research, Conference on Combustion Research in Switzerland, 2017, Zurich, Switzerland

# 8 Publications and presentations

S. Benekos, C.E. Frouzakis, G.K. Giannakopoulos, Y.M. Wright. M. Bolla, K. Boulouchos, Combustion and Flame, 2019 (under review)

E. Mastorakos, P. Allison, A. Giusti, P. De Oliveira, S. Benekos, Y.M. Wright, C.E. Frouzakis, K. Boulouchos, Fundamental Aspects of Jet Ignition for Natural Gas Engines. SAE International Journal of Engines, 2017. 10(5)

P. Kyrtatos, K. Bardis, M. Bolla, A. Denisov, Y. M. Wright, K. Herrmann, K. Boulouchos, Transferability of Insights from Fundamental Investigations into Practical Applications of Prechamber Combustion Systems, 4th International Conference on Ignition Systems for Gasoline Engines, December 6-7, 2018, Berlin

P. Kyrtatos, M. Bolla, S. Benekos, K. Bardis, G. Xu, M. Kotzagianni, Y. M. Wright, G. Giannakopoulos, C. E. Frouzakis, K. Boulouchos, *Advanced Methods for Gas-Prechamber Combustion Research and Model Development*, 16th Conference “The Working Process of the Internal Combustion Engine”, 2017, Graz, Austria

# 9 References


1. Dunn-Rankin, D., *Lean combustion: technology and control*. 2011: Academic Press.
2. Weaver, C.S., *Natural Gas Vehicles - A Review of the State of the Art.* SAE Technical Paper 892133, 1989.
3. Dale, J.D., M.D. Checkel, and P.R. Smy, *Application of high energy ignition systems to engines.* Prog. Energy Combust. Sci., 1997. **23**(5): p. 379-398.
4. Ronney, P.D., *Laser versus conventional ignition of flames.* Opt. Eng., 1994. **33**(2).
5. Sahoo, B., N. Sahoo, and U. Saha, *Effect of engine parameters and type of gaseous fuel on the performance of dual-fuel gas diesel engines -- A critical review.* Renew. Sustain. Energy Rev., 2009. **13(6)**: p. 1151-1184.
6. Schlatter, S., et al., *Comparative Study of Ignition Systems for Lean Burn Gas Engines in an Optically Accessible Rapid Compression Expansion Machine.* SAE Technical Paper 2013-24-0112, 2013.
7. Attard, W.P., et al., *A Turbulent Jet Ignition Pre-Chamber Combustion System for Large Fuel Economy Improvements in a Modern Vehicle Powertrain.* SAE Int. J. Engines, 2010. **3**(2): p. 20-37.
8. Alvarez, C.E.C., et al., *A review of prechamber ignition systems as lean combustion technology for SI engines.* Appl. Thermal Eng., 2018. **128**: p. 107-120.
9. Gussak, L.A., V.P. Karpov, and Y.V. Tikhonov, *The Application of LAG-Process in Prechamber Engines.* SAE Technical Paper 790692, 1979.
10. Toulson, E., et al., *Visualization of Propane and Natural Gas Spark Ignition and Turbulent Jet Ignition Combustion.* SAE Int. J. Engines, 2012. **5**: p. 1821-1835.
11. Baumgartner, L.S., et al., *Investigation of a Methane Scavenged Prechamber for Increased Efficiency of a Lean-Burn Natural Gas Engine for Automotive Applications.* SAE Int. J. Engines, 2015. **8**: p. 921-933.
12. Sakai, Y., et al., *Combustion Characteristics of the Torch Ignited Engine.* SAE Technical Paper 741167, 1974.
13. Brandstetter, W.R., G. Decker, and K. Reichel, *The Water-Cooled Volkswagen PCI-Stratified Charge Engine.* SAE Technical Paper 750869, 1975.
14. Adams, T.G., *Theory and Evaluation of Auxiliary Combustion (Torch) Chambers.* SAE Technical Paper 780631, 1978.

15. Jamrozik, A., *Lean combustion by a pre-chamber charge stratification in a stationary spark ignited engine.* J. Mech. Sci. Techn., 2015. **29**(5): p. 2269-2278.
16. Gentz, G., et al., *Combustion Visualization, Performance, and CFD Modeling of a Pre-Chamber Turbulent Jet Ignition System in a Rapid Compression Machine.* SAE Int. J. Engines, 2015. **8**: p. 538-546.
17. Xu, G., et al., *Characterization of combustion in a gas engine ignited using a small un-scavenged pre-chamber.* Int. J. Engine Res., 2018: p. 1-22.
18. Yamaguchi, S., N. Ohiwa, and T. Hasegawa, *Ignition and burning process in a divided chamber bomb.* Combust. Flame, 1985. **59**(2): p. 177-187.
19. Sadanandan, R., et al., *Detailed investigation of ignition by hot gas jets.* Proc. Combust. Inst., 2007. **31(1)**: p. 719-726.
20. Biswas, S. and L. Qiao, *Prechamber Hot Jet Ignition of Ultra-Lean H$_2$/Air Mixtures: Effect of Supersonic Jets and Combustion Instability.* SAE Int. J. Engines, 2016. **9**: p. 1584-1592.
21. Biswas, S., et al., *On ignition mechanisms of premixed CH$_4$/air and H$_2$/air using a hot turbulent jet generated by pre-chamber combustion.* Appl. Thermal Eng., 2016. **106**: p. 925-937.
22. Allison, P.M., et al., *Pre-chamber ignition mechanism: Experiments and simulations on turbulent jet flame structure.* Fuel, 2018. **230**: p. 274-281.
23. Mastorakos, E., et al., *Fundamental Aspects of Jet Ignition for Natural Gas Engines.* SAE Int. J. Engines, 2017. **10**(5): p. 2429-2438.
24. Roethlisberger, R.P. and D. Favrat, *Investigation of the prechamber geometrical configuration of a natural gas spark ignition engine for cogeneration: Part I. Numerical simulation.* Int. J. Thermal Sci., 2003. **42**(3): p. 223-237.
25. Shah, A., P. Tunestal, and B. Johansson, *Effect of Relative Mixture Strength on Performance of Divided Chamber `Avalanche Activated Combustion' Ignition Technique in a Heavy Duty Natural Gas Engine.* SAE Technical Paper 2014-01-1327, 2014.
26. Hiraoka, K., et al., *Phenomenological 0-Dimensional Combustion Model for Spark-Ignition Natural Gas Engine Equipped with Pre-Chamber.* SAE Technical Paper 2016-01-0556, 2016.
27. Bardis, K., et al., *A Zero Dimensional Turbulence and Heat Transfer Phenomenological Model for Pre-Chamber Gas Engines.* SAE Technical Paper 2018-01-1453, 2018.
28. Ghorbani, A., et al., *Ignition by transient hot turbulent jets: An investigation of ignition mechanisms by means of a PDF/REDIM method.* Proc. Combust. Inst., 2015. **35**(2): p. 2191-2198.
29. Thelen, B.C., G. Gentz, and E. Toulson. *Computational Study of a Turbulent Jet Ignition System for Lean Burn Operation in a Rapid Compression Machine*. in *SAE Technical Paper 2015-01-0396*. 2015.
30. Xu, G., et al., *Experimental and Numerical Investigation of the Engine Operational Conditions' Influences on a Small Un-Scavenged Pre-Chambers Behavior.* SAE Int. J. Eng., 2017. **10(5)**: p. 2414-2428.
31. Bolla, M., et al., *Numerical simulations of pre-chamber combustion in an optically accessible RCEM.* SAE Technical Paper 2019-01-0224, 2019.
32. Bolla, M., et al., *Numerical study of turbulence and fuel-air mixing within a scavenged pre-chamber using RANS and LES.* SAE Technical Paper 2019-01-0198, 2019.
33. Gholamisheeri, M., S. Givler, and E. Toulson, *Large eddy simulation of a homogeneously charged turbulent jet ignition system.* Int. J. Engine Res., 2019. **20**(2): p. 181-193.
34. Male, Q., et al., *Large Eddy Simulation of Pre-Chamber Ignition in an Internal Combustion Engine.* Flow Turbulence and Combustion, 2019. **103**(2): p. 465-483.
35. Feyz, M.E., et al., *Scalar predictors of premixed gas ignition by a suddenly-starting hot jet.* Int. J. Hydrog. Energy, 2019. **44(42)**: p. 23793-23806.
36. Qin, F., et al., *Detailed numerical simulation of transient mixing and combustion of premixed methane/air mixtures in a pre-chamber/main-chamber system relevant to internal combustion engines.* Combust. Flame, 2018. **188**: p. 357-366.
37. Kooshkbaghi, M., et al., *Entropy production analysis for mechanism reduction.* Combust. Flame, 2014. **161**(6): p. 1507-1515.

38. Smith, G.P., et al., *GRI-Mech 3.0*. 2000.
39. Poinsot, T., D. Veynante, and S. Candel, *Quenching processes and premixed turbulent combustion diagrams.* J. Fluid Mech., 1991. **228**: p. 561-606.